University of Alberta

Performance Evaluation of High Bit Rate Cellular Packet Data Systems

by

Carlos Herman Rentel-Gómez

A thesis submitted to the Faculty of Graduate Studies and Research in partial fulfillment of the requirements for the degree of Master of Science

Department of Electrical and Computer Engineering

Edmonton, Alberta

Fall 2002.

National Library of Canada
Acquisitions and Bibliographic Services
395 Wellington Street
Ottawa ON K1A 0N4
Canada

Bibliothèque nationale du Canada
Acquisitions et services bibliographiques
395, rue Wellington
Ottawa ON K1A 0N4
Canada

Your file Votre référence

Our file Notre référence

The author has granted a non-exclusive licence allowing the National Library of Canada to reproduce, loan, distribute or sell copies of this thesis in microform, paper or electronic formats.

L'auteur a accordé une licence non exclusive permettant à la Bibliothèque nationale du Canada de reproduire, prêter, distribuer ou vendre des copies de cette thèse sous la forme de microfiche/film, de reproduction sur papier ou sur format électronique.

The author retains ownership of the copyright in this thesis. Neither the thesis nor substantial extracts from it may be printed or otherwise reproduced without the author's permission.

L'auteur conserve la propriété du droit d'auteur qui protège cette thèse. Ni la thèse ni des extraits substantiels de celle-ci ne doivent être imprimés ou autrement reproduits sans son autorisation.

0-612-81468-8

Canada

University of Alberta

Library Release Form

Name of Author: Carlos Herman Rentel-Gómez

Title of the Thesis: Performance Evaluation of High Bit Rate Cellular Packet Data Systems

Degree: Master of Science

Year this Degree Granted: 2002

Permission is hereby granted to the University of Alberta Library to reproduce single copies of the thesis and to lend or sell such copies for private, scholarly or scientific research purposes only.

The author reserves all other publication and other rights in association with the copyright in the thesis, and except as herein before provided, neither the thesis nor any substantial portion thereof may be printed or otherwise reproduced in any material form whatever without the author's prior written permission.

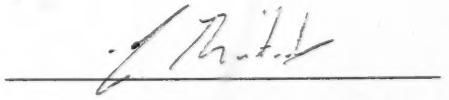

Carlos H. Rentel-Gómez

9525 Genesee Ave. Apartment 232

San Diego, CA 92121 - 1714 USA

July 23rd, 2002

University of Alberta

Faculty of Graduate Studies and Research

The undersigned certify that they have read, and recommend to the Faculty of Graduate Studies and Research for acceptance, a thesis entitled *Performance Evaluation of High Bit Rate Cellular Packet Data Systems by Carlos Herman Rentel-Gómez* in partial fulfillment of the requirements for the degree of Master of Science.

Dr. Witold A. Krzymień

Dr. Ivan J. Fair

Dr. Xiaodai Dong

Dr. Janelle Harms

July 23rd, 2002

Abstract

This thesis presents performance evaluation of high bit rate cellular packet data systems employing adaptive transmission techniques. The performance evaluation is based on the IS-856 (HDR) and 1XTREME systems, both of which have been proposed as an evolution of the 1x cdma2000 cellular standard. Link performance has been estimated by symbol-level simulation of the forward data-traffic channel in the presence of additive white Gaussian noise (AWGN). Link level results are then used in a system level simulator of 19 three-sector cells. The system level simulator uses the standard channel models recommended by the International Telecommunications Union (ITU) in pedestrian and vehicular radio environments. The systems use modulation and code rate adaptation to achieve 1% packet error rate (PER). System performance is evaluated in terms of average sector throughput, packet delay, peak data rate, and fairness metrics. Performance advantages of HDR over 1XTREME are found and analyzed, including an approximate 20% higher average sector throughput in the low-speed pedestrian channel when using the proportionally fair scheduler. Results of this thesis provide useful guidelines for the deployment and better understanding of these new wireless packet data access systems.

Acknowledgements

I would like to thank my supervisor Dr. Witold A. Krzymień for its guidance and support throughout the development of this thesis. I would like to acknowledge the contributions of Miss Ge Li, (University of Alberta/ TR*Labs*) who generated the AWGN PER curves, and Dr. Bahman Darian who contributed with the system level simulation of 1XTREME. Also would like to acknowledge the contributions, and suggestions offered by Dr. Vieri Vanghi (Ericsson Wireless Communications), and Mr. Robert Elliot (University of Alberta/ TR*Labs*).

I am grateful for the financial assistance provided by TR*Labs*, and the University of Alberta, and for the support of the administrative staff in both institutions. Special thanks to my wife for all her sacrifices, and understanding.

To my father and my mother.

TABLE OF CONTENTS

Chapter 1.	**Cellular radio communication**	1
1.1	Introduction	1
1.2	Review of present and future cellular radio standards	7
1.2.1	Advanced mobile phone system (AMPS)	8
1.2.2	Global system for mobile communication (GSM)	8
1.2.3	CDMA digital cellular standard system	9
1.2.4	Third generation standards	11
1.3	Thesis objectives and contributions	14
1.4	Related work	16
1.5	Outline of the thesis	17
Chapter 2.	**High bit rate packet data systems**	18
2.1	Introduction	18
2.2	The HDR system	19
2.2.1	HDR air interface overview	19
2.2.2	Forward link physical layer description	26
2.2.3	Reverse link physical layer description	30
2.2	The 1XTREME system	31
2.3	Summary	32
Chapter 3.	**The cellular radio system environment**	33
3.1	Introduction	33
3.2	Cellular geometric structure	35
3.3	Path-loss and shadow fading model	36
3.4	Multi-path fading model	46
3.5	Summary	52

Chapter 4. Simulation structure and link level simulations 53
4.1 Introduction 53
4.2 General simulation structure 54
4.3 Link level simulations 56
4.3 Structure and functionality of the HDR and 1XTREME Forward links 56
4.3.1.1 HDR forward traffic channel transmission formats 56
4.3.1.2 1XTREME forward shared channel transmission formats 58
4.3.1.3 Turbo encoder and decoder 58
4.3.1.3.1 Turbo encoder 59
4.3.1.3.1.1 Turbo interleaver 61
4.3.1.3.2 Turbo decoder 62
4.3.1.4 Signal constellations and spectrum spreading 65
4.3.1.4.1 HDR forward traffic channel spreading 67
4.3.1.4.2 1XTREME forward shared channel spreading 68
4.3.1.5 Slot and code channel structure 69
4.3.1.5.1 HDR forward channel and slot structure 69
4.3.1.5.2 1XTREME code channel structure 71
4.3.1.6 Hybrid ARQ for HDR 71
4.3.1.7 Soft packet combining and incremental redundancy 73
4.3.1.8 AWGN performance evaluation and its relevance 74
4.3.2 AWGN performance curves 75
4.3.2.1 HDR forward traffic channel PER curves 75
4.3.2.2 1XTREME forward shared channel PER curves 75
4.4 Summary 76

Chapter 5. System level simulation 77
5.1 Introduction 77
5.2 SIR lookup table generation in HDR 79

5.2.1	Power captured by the rake receiver	82
5.2.2	Evaluation of SIR values in the ITU pedestrian A radio channel	85
5.2.3	Evaluation of SIR values in the ITU vehicular B radio channel	87
5.3	MCS format determination	92
5.4	Scheduling of transmissions	93
5.4.1	Round robin scheduler	94
5.4.2	Proportionally fair (PF) scheduler	96
5.5	Packet erasure determination	97
5.6	HDR system level simulator	99
5.7	1XTREME system level simulator	99
5.8	Summary	101
Chapter 6.	**Performance results of HDR and 1XTREME**	103
6.1	Introduction	103
6.2	Distribution of peak Bit Rates over the set of users	104
6.2.1	Pedestrian A channel	104
6.2.1.1	1XTREME	105
6.2.1.2	HDR	106
6.2.2	Vehicular B channel	107
6.2.2.1	1XTREME	107
6.2.2.2	HDR	108
6.3	Distribution of throughput over the set of users	109
6.3.1	Pedestrian A channel	110
6.3.1.1	1XTREME	110
6.3.1.2	HDR	111
6.3.2	Vehicular B channel	112
6.3.2.1	1XTREME	112
6.3.2.2	HDR	113
6.4	Average sector throughput	115

6.4.1	1XTREME	115
6.4.2	HDR	116
6.5	Distribution of delays per user	118
6.5.1	Pedestrian A channel	118
6.5.1.1	1XTREME	118
6.5.1.2	HDR	119
6.5.2	Vehicular B channel	120
6.5.2.1	1XTREME	120
6.5.2.2	HDR	121
6.6	Average delay per sector	122
6.6.1	1XTREME	123
6.6.2	HDR	124
6.7	Number of slots allocated per user	125
6.7.1	Pedestrian A channel	125
6.7.1.1	1XTREME	125
6.7.1.2	HDR	126
6.7.2	Vehicular B channel	127
6.7.2.1	1XTREME	127
6.7.2.2	HDR	128
6.8	Summary	130
Chapter 7	**Conclusion and future research**	131
Bibliography		135
Appendix.	**Link level simulation results**	142
A.1	HDR forward link AWGN channel PER curves	142
A.2	1XTREME forward shared channel AWGN PER curves	153

LIST OF TABLES

Chapter 1. Cellular radio communication 1

1.1 IS-95 parameters 11

Chapter 2. High bit rate packet data systems 18

2.1 HDR forward link transmission formats 23

2.2 HDR parameters 30

2.3 1XTREME forward link transmission formats 31

Chapter 3. The cellular radio system environment 33

3.1 Link budget for the forward Link 39

3.2 Parameters used in cell size computation 39

Chapter 4. Simulation structure and link level simulations 53

4.1 Physical layer packets and rates supported by the HDR forward channel 57

4.2 Physical layer packets and rates supported by the 1XTREME Forward shared channel 58

4.3 Turbo code data bit puncturing pattern 60

4.4 Turbo code tail bit puncturing and repeating pattern 61

Chapter 5. System level simulation 77

5.1 Power and delay profile of the ITU pedestrian A channel 79

5.2 Power and delay profile of the ITU vehicular B channel 80

5.3 Parameters and assumptions of the system level simulation 81

5.4 SIR degradation due to imperfections 91

5.5 SIR require to achieved PER = 1% 94

Chapter 6. Performance results of HDR and 1XTREME 103

6.1 Fairness metric F for the number of slots allocated per user over 16 users per sector 129

Chapter 7 Conclusion and future research 131

7.1 Average throughput per sector for pedestrian A channel, 16 users for slow sector selection for round-robin and proportional fair schedulers 132

LIST OF FIGURES

Chapter 1.	**Cellular radio communication**	1
1.1	Frequency reuse in a coverage area	2
1.2	The cellular network	3
1.3	Multiple access techniques	5
1.4	Hard (a), and soft (b) handoffs	6
1.5	Bandwidth of IS-95 and cdma2000	13
Chapter 2.	**High bit rate packet data systems**	18
2.1	HDR forward link packet transmission	20
2.2.a	HDR normal termination of a packet transmission on the forward link	24
2.2.b	HDR early termination of a packet transmission on the forward link	24
2.3	Slot structure in HDR	27
2.4	HDR forward link traffic/control channel structure	28
2.5	Base-band 1XTREME forward link channel structure	32
Chapter 3.	**The cellular radio system environment**	33
3.1	Cell layout	36
3.2	Antenna gain pattern	40
3.3	Ideal and simulated auto-correlation of Gaussian shadow numbers	45
3.4	Block diagram of the modified Smith channel model method	49
3.5	Pdf of theoretical and simulated correlated Rayleigh numbers	51
3.6	Auto-correlation comparison of theoretical and simulated Rayleigh numbers at 60km/h with fc = 1.9 GHz	51
3.7	Auto-correlation comparison of theoretical and simulated Rayleigh numbers at 3km/h with fc = 1.9 GHz	52

Chapter 4. Simulation structure and link level simulations 53

4.1 General simulation structure of HDR and 1XTREME 54

4.2 Turbo encoder used in HDR and 1XTREME 60

4.3 Interleaver structure 61

4.4 Turbo decoder 63

4.5 Signal constellation for QPSK modulation 65

4.6 Signal constellation for 8PSK modulation 65

4.7 Signal constellation for 16QAM modulation 66

4.8 Signal constellation for 64QAM modulation 66

4.9 HDR forward channel structure 69

4.10 HDR forward channel active slot structure (a) the first slot (b) the non-first slot for multi-slot transmission 70

4.11 HDR forward channel idle slot structure 70

4.12 1XTREME forward shared channel structure 71

4.13 Example of slot interlacing for multi-slot packet transmission in HDR forward channel 72

4.14 HDR forward traffic channel structure in simulation 74

4.15 1XTREME forward shared channel structure in simulation 74

Chapter 5. System level simulation 77

5.1 System-level simulation structure 78

5.2 cdf's of SIR values in ITU ped. A radio environment with slow best sector selection at 3km/h 87

5.3 cdf of SIR values in ITU veh. B radio environment with slow best sector selection at 60km/h 90

5.4 cdf's of estimated SIRs in pedestrian A channel with imperfections 91

5.5 cdf's of estimated SIRs in vehicular B channel with imperfections 92

Chapter 6. Performance results of HDR and 1XTREME 103

6.1 1XTREME distribution of peak bit rates in an embedded sector for 100 drops of 16 users each for the ITU pedestrian A channel with RR scheduler 105

6.2 1XTREME distribution of peak bit rates in an embedded sector for 100 drops of 16 users each for the ITU pedestrian A channel with PF scheduler 105

6.3 HDR distribution of peak bit rates in an embedded sector for 100 drops of 16 users each for the ITU pedestrian A channel with RR scheduler 106

6.4 HDR distribution of peak bit rates in an embedded sector for 100 drops of 16 users each for the ITU pedestrian A channel with PF scheduler 106

6.5 1XTREME distribution of peak bit rates in an embedded sector for 100 drops of 16 users each for the ITU vehicular B channel with RR scheduler 107

6.6 1XTREME distribution of peak bit rates in an embedded sector for 100 drops of 16 users each for the ITU vehicular B channel with PF scheduler 107

6.7 HDR distribution of peak bit rates in an embedded sector for 100 drops of 16 users each for the ITU vehicular B channel with RR scheduler 108

6.8 HDR distribution of peak bit rates in an embedded sector for 100 drops of 16 users each for the ITU vehicular B channel with PF scheduler 108

6.9 1XTREME distribution of throughput per user over the set of users (100 drops of 16 users each) in an embedded sector for ITU pedestrian A channel with RR scheduler 110

6.10 1XTREME distribution of throughput per user over the set of users (100 drops of 16 users each) in an embedded sector for ITU pedestrian A channel with PF scheduler 110

6.11 HDR distribution of throughput per user over the set of users (100 drops of 16 users each) in an embedded sector for ITU pedestrian A channel with RR scheduler 111

6.12 HDR distribution of throughput per user over the set of users (100 drops of 16 users each) in an embedded sector for ITU pedestrian A channel with PF scheduler 111

6.13 1XTREME distribution of throughput per user over the set of users (100 drops of 16 users each) in an embedded sector for ITU vehicular B channel with RR scheduler 112

6.14 1XTREME distribution of throughput per user over the set of users (100 drops of 16 users each) in an embedded sector for ITU vehicular B channel with PF scheduler 112

6.15 HDR distribution of throughput per user over the set of users (100 drops of 16 users each) in an embedded sector for ITU vehicular B channel with RR scheduler 113

6.16 HDR distribution of throughput per user over the set of users (100 drops of 16 users each) in an embedded sector for ITU vehicular B channel with PF scheduler 113

6.17 1XTREME total average throughput per embedded sector as a function of the number of users per drop for 100 drops, RR scheduler 115

6.18 1XTREME total average throughput per embedded sector as a function of the number of users per drop for 100 drops, PF scheduler 116

6.19 HDR total average throughput per embedded sector as a function of the number of users per drop for 100 drops, RR scheduler 116

6.20 HDR total average throughput per embedded sector as a function of the number of users per drop for 100 drops, PF scheduler 117

6.21 1XTREME distribution of delays per delivered packet over the set of users (100 drops of 16 users each) in an embedded sector for ITU pedestrian A channel with RR scheduler 118
6.22 1XTREME distribution of delays per delivered packet over the set of users (100 drops of 16 users each) in an embedded sector for ITU pedestrian A channel with PF scheduler 119
6.23 HDR distribution of delays per delivered packet over the set of users (100 drops of 16 users each) in an embedded sector for ITU pedestrian A channel with RR scheduler 119
6.24 HDR distribution of delays per delivered packet over the set of users (100 drops of 16 users each) in an embedded sector for ITU pedestrian A channel with PF scheduler 120
6.25 1XTREME distribution of delays per delivered packet over the set of users (100 drops of 16 users each) in an embedded sector for ITU vehicular B channel with RR scheduler 120
6.26 1XTREME distribution of delays per delivered packet over the set of users (100 drops of 16 users each) in an embedded sector for ITU vehicular B channel with PF scheduler 121
6.27 HDR distribution of delays per delivered packet over the set of users (100 drops of 16 users each) in an embedded sector for ITU vehicular B channel with RR scheduler 121
6.28 HDR distribution of delays per delivered packet over the set of users (100 drops of 16 users each) in an embedded sector for ITU vehicular B channel with PF scheduler 122
6.29 1XTREME average delay per delivered packet in an embedded sector as a function of the number of users per drop for 100 drops, RR scheduler 123
6.30 1XTREME average delay per delivered packet in an embedded sector as a function of the number of users per drop for 100 drops, PF scheduler 123

6.31 HDR average delay per delivered packet in an embedded sector as a function of the number of users per drop for 100 drops, RR scheduler 124
6.32 HDR average delay per delivered packet in an embedded sector as a function of the number of users per drop for 100 drops, PF scheduler 124
6.33 1XTREME distribution of the number of slots allocated per user over the set of users (100 drops of 16 users each) in an embedded sector for ITU pedestrian A channel with RR scheduler 125
6.34 1XTREME distribution of the number of slots allocated per user over the set of users (100 drops of 16 users each) in an embedded sector for ITU pedestrian A channel with PF scheduler 126
6.35 HDR distribution of the number of slots allocated per user over the set of users (100 drops of 16 users each) in an embedded sector for ITU pedestrian A channel with RR scheduler 126
6.36 HDR distribution of the number of slots allocated per user over the set of users (100 drops of 16 users each) in an embedded sector for ITU pedestrian A channel with PF scheduler 127
6.37 1XTREME distribution of the number of slots allocated per user over the set of users (100 drops of 16 users each) in an embedded sector for ITU vehicular B channel with RR scheduler 127
6.38 1XTREME distribution of the number of slots allocated per user over the set of users (100 drops of 16 users each) in an embedded sector for ITU vehicular B channel with PF scheduler 128
6.39 HDR distribution of the number of slots allocated per user over the set of users (100 drops of 16 users each) in an embedded sector for ITU vehicular B channel with RR scheduler 128
6.40 HDR distribution of the number of slots allocated per user over the set of users (100 drops of 16 users each) in an embedded sector for ITU vehicular B channel with PF scheduler 129

Appendix. Link level simulation results 142

A.1 HDR PER vs. Es/No curves in AWGN for transmission formats 1-8 142

A.2 HDR PER vs. Es/No curves in AWGN for transmission formats 9-16 143

A.3 HDR PER vs. Es/No curves in AWGN for transmission formats 17-24 144

A.4 HDR PER vs. Es/No curves in AWGN for transmission formats 25-31 145

A.5 HDR PER vs. Es/No curves in AWGN for transmission formats 32-37 146

A.6 HDR PER vs. Es/No curves in AWGN for transmission formats 38-41 147

A.7 HDR PER vs Es/No curves in AWGN for rates 76.8kb/s to 122.88 kb/s with maximum number of slots = 8, and 16 148

A.8 HDR PER vs Es/No curves in AWGN for rates 153.6 And 204.8 with maximum number of slots = 4, 8, and 16 149

A.9 HDR PER vs. Es/No curves in AWGN for rate 307.2 kb/s with maximum number of slots = 2, 4, 8, 16, and packet sizes 1,024 and 2,048 150

A.10 HDR PER vs. Es/No curves in AWGN for rate 614.4 kb/s with maximum number of slots = 1, 2, 4, 8, 16, and packet sizes 1,024 and 2,048 151

A.11 HDR PER vs. Es/No curves in AWGN for rate 1,228.8 kb/s with maximum number of slots = 1, 2, 4, and packet sizes 2,048 and 4,096 152

A.12 1XTREME PER vs. Es/No curves in AWGN for the Forward Shared channel 153

ABBREVIATIONS

1XEV-DO	1x Evolution Data-Only
1XEV-DV	1xEvolution Data-Voice
2G	Second Generation Cellular Systems
3G	Third Generation Cellular Systems
ACK	Acknowledgement
AMC	Adaptive Modulation and Coding
AWGN	Additive White Gaussian Noise
cdf	Cumulative Distribution Function
CDMA	Code Division MultipleAccess
DRC	Data Request Channel
DSL	Digital Subscriber Line
FDD	Frequency Division Duplex
H-ARQ	Hybrid Automatic Repeat Request
HDR	High Data Rate system
IDFT	Inverse Discrete Fourier Transform
IP	Internet Protocol
IS-2000	Interim Standard 2000 (cdma2000)
ISI	Inter-symbol Interference
ITU	International Telecommunications Union
MAC	Medium Access Control
MCS	Modulation and Coding Scheme
N-ACK	Negative-Acknowledgment
OQPSK	Off-set Quadrature Phase-Shift Keying
pdf	Probability Density Function
PER	Packet Error Rate
PF	Proportionally Fair
PN	Pseudo Noise
PPP	Point-to-Point Protocol
QAM	Quadrature Amplitude Modulation
QPSK	Quadrature Phase-Shift Keying
RR	Round Robin
RRM	Radio Resource Management
SBSS	Slow Best Sector Selection
SIR	Signal to Interference Ratio
TDD	Time Division Duplex
TDM	TimeDivision Multiplexing
W-CDMA	Wide-Band CDMA

LIST OF SYMBOLS

$\Phi(n)$	Auto-correlation function
σ	Standard deviation
Es / No	Symbol energy-to-noise power spectral density ratio
$f_{D\max}$	Maximum Doppler frequency
d_{dec}	De-correlation distance
Ω_p	Total average received signal power
L_{rs}	Roof-top-to street diffraction loss
L_{msd}	Multi-screen diffraction loss
L_{bf}	Free space path-loss
L	Path loss
G_b	Antenna gain
P_t	Transmission power per sector
h_b	Base station antenna height
h_m	Mobile terminal antenna height
b	Building separation
w	Street width
H	Average roof-top height
$\overline{P}_i$	Small-scale average power received by i^{th} mobile
R_i	Random variable with Rayleigh distribution
I_i	Interference received by i^{th} mobile
ξ	First order recursive filter coefficient
ν	Gaussian random variable with auto-correlation different than zero

Chapter 1

Cellular radio communication

1.1 Introduction

Initially, radio communications were carried out utilizing high powered, high mounted base stations and big portable radios to provide voice communication services. The idea was to offer a maximum coverage and a good quality of the radio signal; the allocated frequency spectrum was used only by a few channels, and therefore, the radio spectrum was not efficiently used in terms of users served per frequency allocation. The advent of more efficient and smaller semiconductors and integrated circuits reduced the size and cost of portable radios, expanding the corporate based market of radio communications to the general public. The original radio communication system needed an improvement in terms of capacity and spectrum efficiency in order to take advantage of a potentially large market.

The initial solution to this capacity and spectrum efficiency problem is known as the cellular concept [1]. The cellular concept is the basis of all present cellular systems and it represents a major achievement in the radio communications field.

The main idea behind the cellular concept is that of frequency reuse depicted in Figure 1.1; here the total coverage area is divided into imaginary regions in space

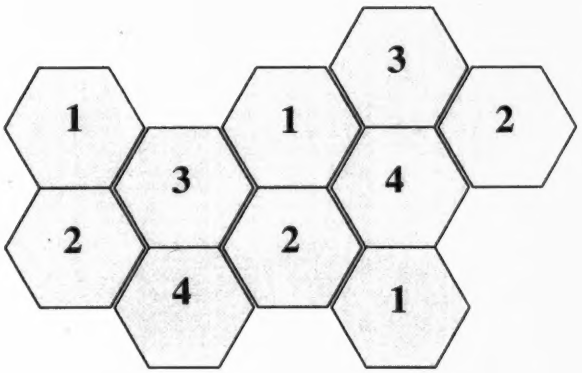

Figure 1.1. Frequency reuse in a coverage area.

called cells (which are drawn as hexagons in Figure 1.1 for the purpose of illustration, but in reality have different shapes due to radio propagation considerations). The first cellular systems comprised cells which serve a region in space with a low powered base station utilizing part of the allocated frequency spectrum; neighboring cells used different portions of the allocated spectrum, and cells separated by a considerable distance reuse the same set of frequencies. The reuse of the frequencies is possible if the separation of both regions in space is large enough to cause the mutual interfering signals to be at a tolerable level. The development of the cellular concept provided the necessary steps toward the materialization of the first generation of cellular systems which are still in use mainly in South and North America.

The classical cellular network architecture (Figure 1.2) is based on the cellular concept. Each cell is served by a base transceiver station (BTS) and the BTSs are

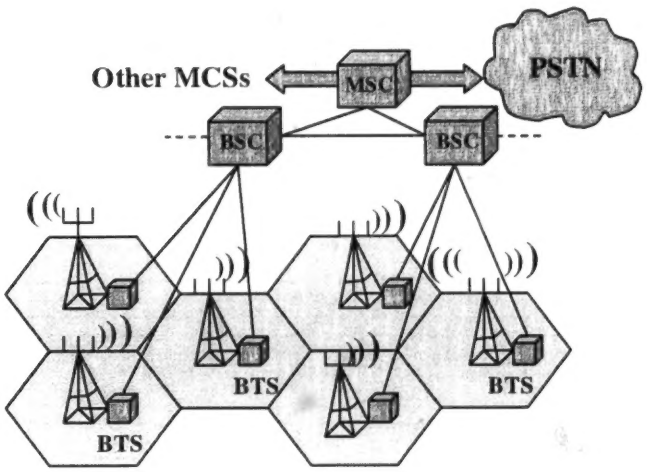

Figure 1.2. The cellular network.

connected to a base station controller (BSC) which in turn is connected to other BSCs and the central unit called the mobile switching center (MSC). The MSC handles the interconnection of the mobile stations with each other and with the Public Switched Telephone Network (PSTN), and it is also responsible along with the BSCs for ensuring uninterrupted communication throughout the entire region covered . The region between the base station and the mobile station is called the air-interface, and the network that supports over the air-interface connections is called the core network. Mobile terminals are also part of the cellular network (not shown in Figure 1.2)

The base station's main function is to serve the mobile stations as a point of interface between the air-interface and the core network. It is the point where users access different services provided by the cellular network.

Multiple access techniques are used to divide the radio resource among the users. Three multiple access techniques are commonly employed in cellular systems: frequency-division multiple access (FDMA), time-division multiple access (TDMA), and code- division multiple access (CDMA). In FDMA the allocated frequency band is sub-divided into smaller sub-bands (Figure 1.3-a); each sub-band is permanently assigned to a particular user that accesses the system for the total duration of the connection. More efficient variations to this technique are employed, in which the sub-bands are temporarily assigned to low priority services (low bit rate packet data transmissions) and hopped to a different sub-band when higher priority services try to access the system. This former technique is employed in the Cellular Digital Packet Data (CDPD) system [2]. In TDMA (Figure 1.3-b) several users share a common sub-band at different ordered time slots, and in CDMA (Figure 1.3-c), all users utilize the same allocated spectrum at the same time; the different transmissions are separated by different orthogonal and/or semi-orthogonal codes embedded to the transmitted signals [3]. Hybrids of these multiple access techniques are usually used in real systems such as FDMA/CDMA, TDMA/CDMA or FDMA/TDMA, the later used in most so-called TDMA systems (i.e., GSM, IS-136, PDC etc). Another multiple access technique that has gained some attention recently is space-division multiple

access (SDMA), where the transmissions to multiple users are separated in space by controlling the radiation of the base station antennas.

It is necessary to ensure uninterrupted communication when the user is moving from one access point into a neighboring one. The process of handing over a user from one access point to another is known as handoff.

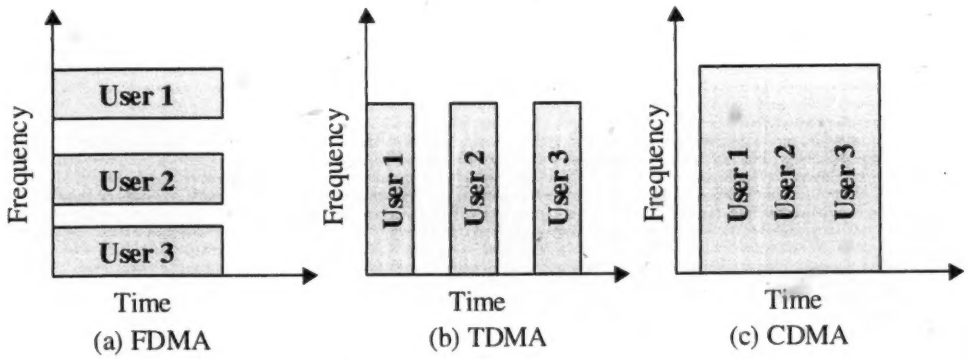

Figure 1.3. Multiple access techniques.

There are different types of handoffs depending on the mode of operation and the system where they are employed [4].

The two most representative types of handoffs are hard handoff, and soft handoff.

Hard handoff (Figure 1.4-a) occurs when the mobile station is transferred to a new access point by first breaking the connection with the old access point. It is a break before make connection over the air-interface.

Soft handoff (Figure 1.4-b) is a make before break transfer of a mobile station over the air-interface. During the execution of this handoff, the mobile station is connected to at least two access points at the same time before breaking with the old access point.

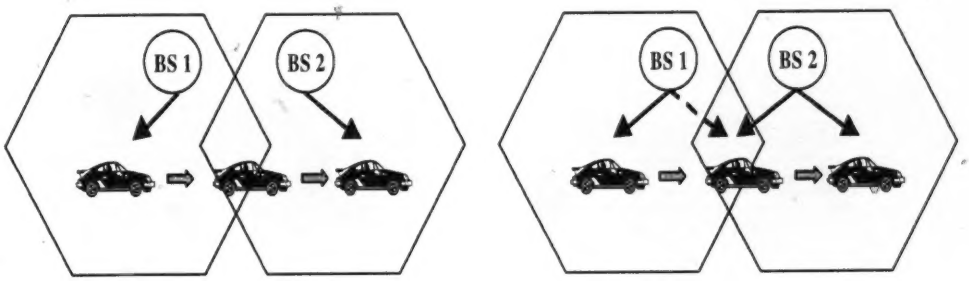

(a) Hard handoff (b) Soft handoff

Figure 1.4. Hard (a), and Soft (b) Handoffs.

In order to achieve an efficient operation of the cellular network, it is also necessary to control the power emitted by the mobile and base station transmitters. The primary reason for this is to ensure a minimum acceptable signal to interference ratio (SIR) of the received signal by off-setting the attenuation caused by the variable distance separation between the transmitter and the receiver. Power control helps to increase battery life and the capacity (users/cell) of the system.

Power control is particularly important in CDMA systems, where all users are transmitting in the same frequency band, and hence all interfere with one another. In CDMA systems, power control is also used to keep the mean powers of all received signals at the base station at the same level; this not only increases

capacity, but also reduces the *near-far* problem. The *near-far* problem in CDMA occurs when two users are simultaneously transmitting with the same power to a base station receiver; the user closer to the base station can effectively capture the receiver leaving the other user without service. In order to solve the *near-far* problem, the system has to control the transmitted powers of the mobiles, so that they reach the base station with equal mean powers.

Radio resource management (RRM) is another important system level concept in cellular radio systems. Once a band of frequencies is allocated for the use of radio communications in a cell or a particular region, it is desirable to make efficient use of it among the multiple users trying to access the common service access point (i.e., base station). RRM primary objectives are to guarantee a desired quality of service and provide continuous support of the multiple radio connections throughout the entire coverage region. RRM primary functions are to allocate and if necessary re-allocate channels for the connections, selection of the best service access point for the connections, and congestion control. RRM relies on multiple access techniques, handoff, and power control.

1.2 Review of present and future cellular radio standards

Presently deployed cellular systems constitute what is called the first and second generation of cellular systems; from these groups the most representative standards are, the Advanced Mobile Phone System (AMPS), Global System for Mobile Communications (GSM), and the CDMA digital cellular standard IS-95. Future cellular radio standards known as third generation (3G) systems are now

fully specified. The initial deployment of the 1x (1.25 MHz) version of the IS-2000 system began already in 2001in the U.S and Korea. Similarly, the initial deployment of the 5 MHz W-CDMA system began in 2001 in Japan. This section provides a brief overview of these systems with emphasis on the IS-95 and IS-2000 systems.

1.2.1 Advanced mobile phone system (AMPS)

The AMPS system belongs to the first-generation (1G) of cellular systems, it was developed in AT&T Bell laboratories with the idea to provide voice services only. It was first deployed in Chicago in 1983 by Ameritech [5]. AMPS is an analog system using frequency modulation (FM), and FDMA as the multiple access technique. Each channel occupies a 30 kHz bandwidth of a total of 832 possible channels, and frequency division duplex (FDD) is used to separate the transmission and reception paths of every full-duplex channel. AMPS is still used in South and North America, but its use has started to decline mainly due to the competition from second-generation systems that provide more services with better quality, more capacity, and lower cost of deployment and of mobile terminals.

1.2.2 Global system for mobile communications (GSM)

GSM is the second-generation cellular system (2G) standard with more subscribers worldwide. It was first introduced in Europe in 1991 in order to serve as a Pan-Eropean cellular system. GSM uses digital modulation with hybrid

TDMA/FDMA, and each channel bandwidth is 200 kHz. The services provided are divided in three groups [6].

- Telephone service;
- Bearer service for the provision of data services up to 9.6 kb/s; it includes the support of packet switching protocols, and automatic request for retransmission (ARQ) for error detection;
- Supplementary services include number identification services, call forwarding, multiparty services, call restriction services etc.

GSM represents an evolution of 1G systems due mainly to the digital services provided, and its network architecture.

1.2.3 CDMA digital cellular standard IS-95

CDMA IS-95 was adopted as a U.S digital cellular standard in 1993 by the Telecommunications Industry Association (TIA). IS-95 is a dual mode system that provides a digital cellular service through spread-spectrum techniques [7]; it also provides first generation analog service to ease the transition from first to second generation cellular systems.

The network structure of the IS-95 system is the same as the classical network previously depicted in Figure 1.2, with an MSC that controls and handles the radio connections, interface with the PSTN, and base stations that serve as points of access for the mobile stations to the cellular services. The path from the mobile station to the base station is called the *reverse link*, and the path from the base station to the mobile is called the *forward link*. A number of different radio

channels are specified per link. In the forward link they include, the pilot, synchronization, paging, and traffic channel. In the reverse link they include, the access, and traffic channels. Traffic channels are used to convey voice or data to or from an individual mobile station. The pilot channel is used as a reference for coherent detection at the mobile station receiver, paging channels are used to signal a mobile station of an incoming call, and the sync channel is used by the mobile station to acquire system time synchronization. Table 1.1 shows the most important parameters of the IS-95 air interface standard.

IS-95 forward link

The forward link of the IS-95 system consists of up to 61 traffic channels, up to 7 paging channels, 1 sync channel, and 1 pilot channel. All channels are orthogonally multiplexed to a common RF carrier using Walsh functions [8]. The different base station transmissions are separated by different offsets of the same short pseudo noise (PN) sequence. Hence, channelization in the forward link is achieved by a combination of orthogonal Walsh functions and short PN sequences. The Walsh covered symbols quadrature-modulate a short PN sequence before transmission in a form of QPSK modulation of the RF carrier.

IS-95 reverse link

The reverse link of IS-95 consists of traffic channels, and access channels. Channelization on the reverse link is achieved by different phase shifts of a long PN code sequence, the different phase shifts are obtained by masking of a 0 offset PN sequence, the mask is partially derived from the electronic serial number

(ESN) of the mobile terminal. Therefore separation of different transmissions on the reverse link is achieved by means code multiplexing. Modulation on the reverse link is by means of an 64-ary orthogonal modulation in base-band, and OQPSK modulation of the RF carrier.

Bandwidth	1.25 MHz
Chip rate	1.2288 Mchips/s
Frequency band reverse link	869-894 MHz 1930-1980 MHz
Frequency band forward link	824-849 MHz 1850-1910 MHz
Bit rates for data services	Rate set 1: 9.6 kb/s Rate set 2: 14.4 kb/s IS-95B: 115.2 kb/s
Soft handoff	Yes
Power control	Reverse link: open loop + closed loop (fast) Forward link: closed loop (slow)
Modulation	Forward link: QPSK Reverse link: OQPSK
Speech code	8, 13 kb/s
Frame length	20 ms
Error control coding	Convolutional codes (constraint length = 9, forward link code rate = 1/2 or 3/4, reverse link code rate = 1/3 or 1/2)

Table 1.1 IS-95 parameters [9].

1.2.4 Third generation standards

First and second generation cellular systems were primarily designed for voice and low data rate services. 3G systems are designed to improve 2G voice services, and include multimedia services and wireless Internet access. In the International Telecommunications Union (ITU), the 3G cellular systems are called International Mobile Telecommunications-2000 (IMT-2000). The objectives of the IMT-2000 systems are

- Flexibility to include new services;
- Provide data rates up to 384 kb/s for high mobility environments;
- Provide data rates up to 2 Mb/s for low mobility environments;
- High spectrum efficiency in comparison to 2G systems.

It has been recognized that a unified approach to a ubiquitous global 3G system is not possible at this time [9], and that some future 3G systems will evolve from the different 2G systems in existence. 2G systems based on GSM will evolve through the Enhanced Data for GSM Evolution (EDGE) system, and the General Packet Radio Service (GPRS) core network for packet switched services [10,11]. EDGE and GPRS use the GSM network infrastructure.

2G systems based on the IS-95 cellular standard will evolve through cdma2000 for the circuit switched and medium data rate services. For packet switching services at high data rates (up to 2Mb/s), several systems have been proposed including High Data Rate (HDR) system by Qualcomm Inc. [12, 13] and 1XTREME by Motorola and Nokia [14]. These systems are called 1x Evolution Data-Only (1xEV-DO) and 1x Evolution Data-Voice (1xEV-DV) respectively. These systems are aimed to provide higher data rates than 3G solutions designed around circuit switched technology. The specifics of the data optimization techniques utilized by these systems will be explained in later chapters. 1xEV-DO is a separate standard called IS-856.

Cdma2000 is a solution that utilizes a multi-carrier forward link with in principle up to 12 parallel CDMA carriers of 1.25 MHz each, and the same chip rate as that of IS-95 (see Table 1.1). Direct-spread with chip rate of 3.6864

Mchips/s is used on the reverse link. The first release will be deployed with one carrier (a 1X mode), see Figure 1.5 for 3x mode version of this system.

A new system standard has also been developed for future new service providers called WCDMA [15]. WCDMA uses 5 MHz bandwidth on both the forward and reverse links; two versions of channel duplexing are specified, time division duplex (TDD), and frequency division duplex (FDD) [16].

The major technical improvements of 3G systems with respect to 2G systems are

- Fast forward link power control;
- Improved error correction techniques for data transmission (Turbo coding);
- Pilot channel on the reverse link for coherent demodulation;
- Wider bandwidth;
- Optimized packet switched network for high bit data rate transmission;
- Capacity enhancement enabling techniques such as smart-antennas [17].

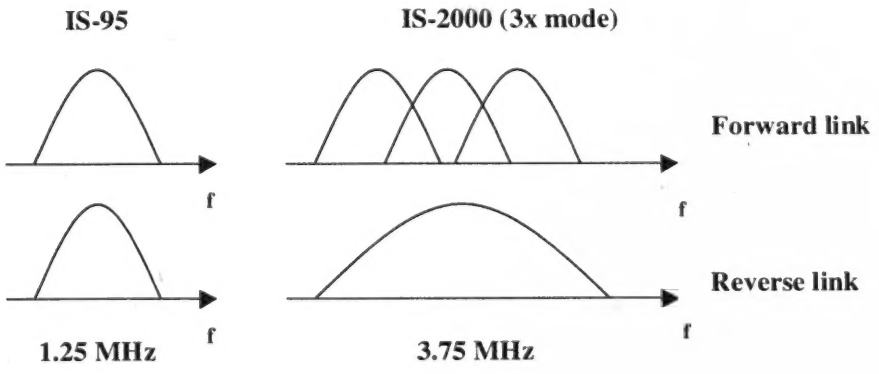

Figure 1.5. Bandwidths of IS-95 and cdma2000 (a possible configuration).

Beyond 3G cellular systems, a seamless Internet Protocol (IP) core network is envisioned, providing services between different wireless and wired applications. A user may have access to different systems adapted to a particular need and environment through a common packet switched platform [18, 19]. Future cellular radio systems will provide even higher capacities and higher data rates for future services.

1.3 Thesis objectives and contributions

The primary objective of this research work is to analyze the forward link performance of high bit-rate packet data systems designed as an evolution of the IS-2000 system through the development of a system level simulator, with emphasis on the 1xEV-DO system or HDR. The entire system will be modeled under different radio environments and system level assumptions to compute performance metrics that will help to understand its capabilities and limitations. The system level simulator will be useful for the future study of RRM algorithms, scheduling algorithms, and network optimization techniques.

The specific contributions of this research work are

- A complete modeling of the radio environment of a cluster of 19 tri-sectored cells is carried out; vehicular and pedestrian environments are considered following the recommendations of the International Telecommunications Union (ITU) for the evaluation of radio transmission

technologies for IMT-2000 [20]. Measured antenna data are used to model the antenna gain-pattern in the simulation.

- Link level simulation results are presented for all HDR and 1XTREME transmission formats in order to use them in the system level simulator. The link level simulation results are obtained in an additive white Gaussian noise (AWGN) channel due to the very small slot size in the system (1.67ms and 5ms) that causes the channel to be practically time-invariant during a single-slot packet transmission.
- Scheduling of the transmissions is important to ensure optimum utilization of the radio resources, and fairness among the users accessing a system; two scheduling mechanisms are evaluated; a modified round robin scheduler, and a proportionally fair (PF) scheduler.

The following metrics are used for the comparative performance evaluation:

- Distribution of bit rates over the set of users
- Distribution of average throughput over the set of users
- Average throughput per sector
- Distribution of delays over the set of users
- Distribution of average delay over the set of users
- Average delay per sector
- Distribution of the number of allocated transmission slots per user.

1.4 Related work

System level simulators have been developed before for the performance analysis of 3G cellular radio systems. In [21] an advanced WCDMA system level simulator has been developed, in which traffic and mobility of the users are simulated using statistical models specified in [22]. Another WCDMA system level simulator has been described in [10], where the authors model the mobility of the users by adding the speed-dependant time-correlation to the fading signals generated, calling this procedure a semi-static approach.

In [23], the authors provided simulation results for the average throughput in one sector of the central cell of a cluster of 19 cells for the HDR system. The results are shown for 6, 3, and Omni-sector deployments, and for 1 and 2 access terminal (mobile station) antennas. The advantage of multi-user diversity is identified with the use of the proportionally fair scheduler over the round robin scheduler. No effects on the throughput due to speed, or specific radio environment are presented, and additional important metrics such as fairness, delays or data rates achieved are not discussed.

In [24], 1XTREME forward link level simulation results are presented and the average sector throughput is calculated for vehicle speeds of 0 and 3 km/hr. Two schedulers are presented. The *equal average power* scheduler equalizes the number of frames assigned to each user for transmission, and the *equal average data* scheduler equalizes the amount of data delivered to all users. The former scheduler is used to avoid the unfair situation occurring in the latter in which one

user close to the serving base station can get higher data rates than another user farther away.

1.5 Outline of the thesis

A system level simulator for the IS-2000 compatible high bit-rate packet data systems has been developed and performance results have been obtained and presented with different system level assumptions.

Chapter 2 presents a description of the air-interface, physical layer, and design principles behind the high bit-rate packet data systems for IS-2000, with especial emphasis on the HDR system.

Chapter 3 addresses the cellular radio environment assumptions used in this research work; path-loss model, large and small scale fading models are presented and justified.

Chapter 4 describes the link level simulation procedure and presents the results.

Chapter 5, The structure of the system level simulator is presented along with the channel predictor, the schedulers, and the best sector selection methods.

Chapter 6, The performance results are discussed; throughput, delay, and fairness metrics are obtained and analyzed under different radio environments and system level assumptions.

Chapter 7 Presents the conclusions of this research work and future research directions are suggested.

Chapter 2

High bit-rate packet data systems

2.1 Introduction

HDR and 1XTREME have been proposed for standardization as evolution of the existing 3G IS-2000 standard [25], [12]. These systems are known as the 1xEvolution of IS-2000 and are expected to provide high packet data rate services for nomadic users [26]. The nomadic user expects to be able to access the same *Home* data services while he/she is traveling or has reached his/her final destination. It would be desirable to access the data services independently of location or motion, and the performance of the services provided should at least equal those of the present cable or DSL wire-line systems. 1xEvolution systems try to fill the present gap of an efficient high data rate wireless system through the use of data optimization techniques such as: packet switching and data rate adaptation.

The 1xEvolution systems take advantage of the radio frequency equipment and base stations already deployed of the IS-95 cellular digital network to provide the adequate coverage; 1xEvolution terminals will differ only in their base-band

processing portion. The network architecture is expected to follow an Internet-Protocol structure, with the ultimate intention of implementing Mobile IP.

This chapter offers a description of the 1xEvolution systems with special emphasis on HDR. Section 2.2 addresses the air-interface, physical layer, and network architecture descriptions of HDR. Section 2.3 presents a brief description of the 1XTREME system.

2.2 The HDR system

Most of our description will be focused on the forward link since it is expected that most of the data services provided will have a highly asymmetrical behavior [9] (i.e., most of the data traffic will flow from the network to the mobile terminal).

2.2.1 HDR air-interface overview

Recognizing that the requirements of data and voice are very different in terms of delay constrain, bandwidth utilization, and traffic characteristics, the HDR system's first fundamental design principle is to separate voice from data services by using non-overlapping frequency spectrum allocations. The 1.25 MHz IS-95 or 1x cdma2000 RF carrier can provide voice and low/medium rate data services, and a separate carrier with the same RF components as the IS-95 system is used exclusively for the high bit-rate data services provided by HDR. The separation of the services is a natural choice since optimization of radio resource utilization is less effective when very different services are sharing a common frequency band at the same time. A high bit-rate data user can take much more

bandwidth and power resources from a network than a voice user, therefore, its requirements in terms of coverage and quality of service are quite different, making it difficult to optimize a single network for both services.

The forward link packet transmissions of the different users are time-multiplexed as shown in Figure 2.1; and the base station transmits at the maximum power at all times. The pilot signal is not continuously beaming on the forward link, since it is also time division multiplexed with the data; this allows for the reduction of the interference when packets of a given user are not being transmitted in a different sector.

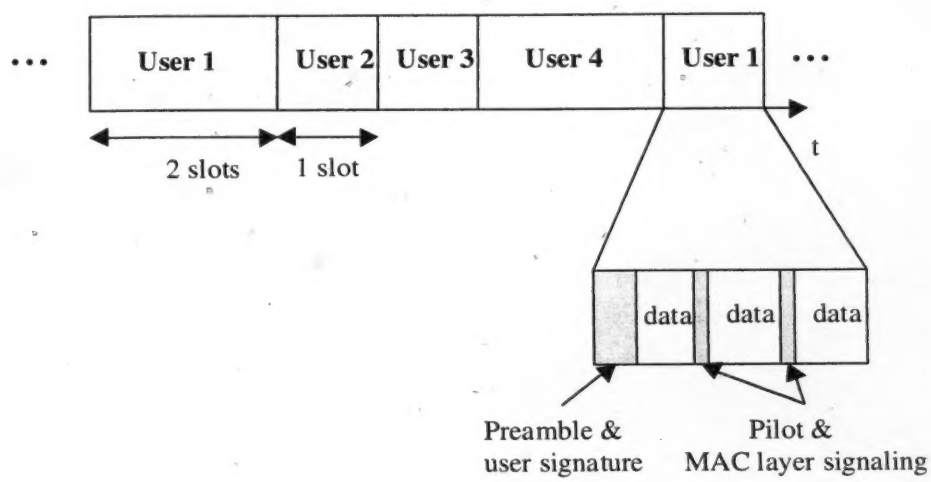

Figure 2.1. Forward link packet transmission.

The preamble is sent at the beginning of every packet transmission attempt in order to assist the mobile terminal with synchronization and identification of the

data packet. (The preamble in HDR is covered by a specific Walsh cover or MAC index)

The wireless channel is characterized by rapid variations of signal power caused by multi-path fading and Doppler frequency shifts [26]. These features make the wireless channel a very unfriendly environment for the transmission of information. Techniques to combat fading are necessary in order to be able to successfully transmit information through a wireless channel.

Transmission on the forward link of HDR is enhanced through the use of adaptive modulation and coding (AMC) and hybrid-automatic repeat request (H-ARQ) techniques, [27], [28], [29], [30]. AMC takes advantage of the time-varying nature of the fading channel to change the modulation and coding rate of the transmitted signal. More bandwidth efficient modulations (e.g., larger constellation sizes) and higher code rates are used when the signal experiences a boost in power, and more robust modulation (e.g., smaller constellation size) and lower code rates are used during fades of the signal. Since the fading signal experiences actually wider peaks than deep fades, the adaptive technique provides higher efficiency and higher data rates.

The modulation and coding rate formats used in HDR are presented in Table 2.1. The information of the transmission format to be used, and the *best* sector that should transmit the data is sent from the mobile to the base station through the Data Rate Control (DRC) channel. The DRC indicates through a 4 bit symbol, which one of the 12 possible transmission formats the selected sector is going to use to transmit the packets to the particular user. The DRC symbols are covered

with a specific Walsh function; each Walsh function represents a particular sector of the active set that is chosen as the transmitting sector [31].

A Type II Hybrid-Automatic Repeat Request (H-ARQ) scheme is used on the forward link to further decrease the error rate of the air-interface and maximize throughput [32]. A packet is transmitted in one slot of 1.67 ms of duration on the data traffic channel. The mobile terminal sends an acknowledgement message on the ACK channel of the reverse link if the packet is decoded successfully, otherwise it sends a negative acknowledgement message and the packet is re-transmitted. The Type II H-ARQ is a technique that adapts to the changing conditions of the radio channel by utilizing incremental redundancy and packet combining. In the simplest form of incremental redundancy the transmitter responds to re-transmission requests by sending additional parity bits to the receiver. The receiver appends these additional parity bits to the original packet received, effectively increasing the decoding power of the decoder. The combining of the re-transmitted packets; the noisy packets (i.e., packets not-successfully decoded) in one transmission are not discarded but *soft* combined with future noisy packets to effectively decode the packet.

Code combining is a technique that is more effective in high-interference environments where the classical ARQ scheme of repeating the transmission of a packet until a good one is received, fails. Soft combining implies that soft samples of corresponding bits of packets transmitted in different slots are combined, using e.g. maximal ratio combining. In HDR both incremental redundancy and soft packet combining are used. Soft combining is performed whenever an encoded bit

of a packet is received again (the same bit has been received already at least once in earlier packet transmissions).

Format	Data rate (kb/s)	Max. no. of slots	Modulation	Code rate	Packet size (bits)
1	38.4	16	QPSK	1/5	1,024
2	76.8	8	QPSK	1/5	1,024
3	153.6	4	QPSK	1/5	1,024
4	307.2	2	QPSK	1/5	1,024
5	614.4	1	QPSK	1/5	1,024
6	307.2	4	QPSK	1/3	2,048
7	614.4	2	QPSK	1/3	2,048
8	1,228	1	QPSK	1/3	2,048
9	921.6	2	8PSK	1/3	3,072
10	1,843	1	8PSK	1/3	3,072
11	1,228.8	2	16QAM	1/3	4,096
12	2,476.6	1	16QAM	1/3	4,096

Table 2.1. HDR forward link transmission formats [31].

The SIR values computed in the mobile terminal are subject to errors of prediction and measurement, therefore the mapping of predicted SIR values to formats in Table 2.1 has to be conservative in many cases in order to achieve a

desired packet error rate performance. The conservative nature of the mapping can affect the maximum throughput achievable by the connections due to excess SIR values (i.e., higher than expected SIR values) [33]. The H-ARQ scheme takes advantage of excess SIR values by acknowledging the packets transmitted before the maximum number of slots is reached. The H-ARQ technique can effectively increase the data rate and maximize throughput. The specific mapping table from SIR values to formats is presented in chapter 6.

The transmission of a packet in one of the formats can take a maximum number of slots for re-transmission as specified in the third column of Table 2.1. Figure 2.2-a shows the case where the transmitted packet is acknowledged before the maximum number of slots for re-transmission are used, in this case the packet has been effectively sent in fewer slots than expected, and hence higher data rate has been achieved.

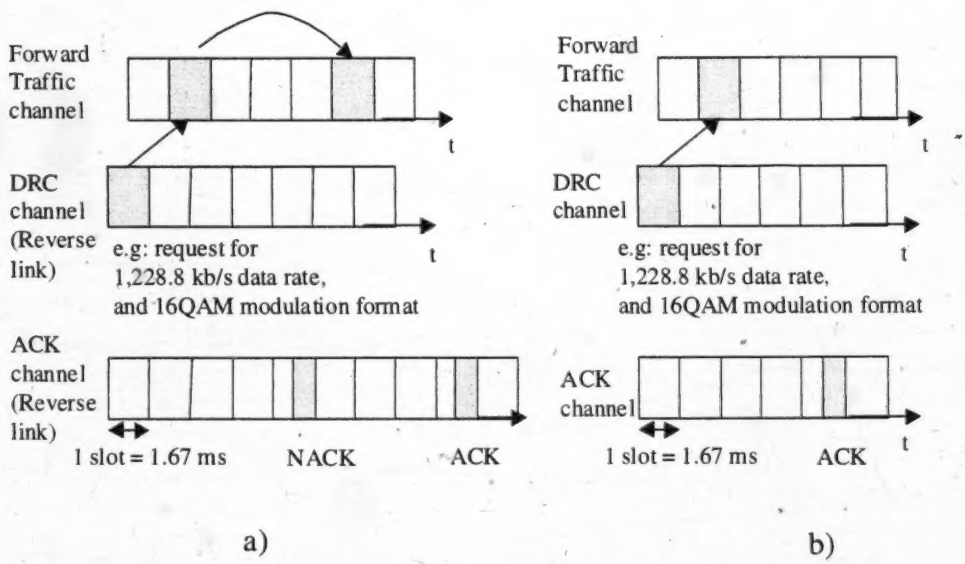

Figure 2.2. a) *Normal* termination of a packet transmission on the forward link (data rate achieved = 1,228.8 kb/s); b) Early termination of a packet transmission on the forward link (data rate achieved = 2,457.6 kb/s)

Figure 2.2-b depicts the case where the packet uses the maximum number of re-transmission slots; in this case the rate of transmission of the packet is the one specified in the second column of Table 2.1 for any specific format used. In all cases the re-transmission of a packet occurs at every fourth slot to allow for time-diversity and give time to decode a packet and transmit the acknowledgment to the corresponding sector.

In order for Type II H-ARQ schemes and the format of transmission adaptation technique to work properly, it is necessary to estimate the channel-state at the receiver for channel prediction and format of transmission determination. In HDR the mobile terminal estimates the channel condition by measuring the received signal to interference ratio (SIR) from the pilot signal. The value of SIR is then mapped to a transmission format that the forward link connection can support with adequate error performance. The mapping from a channel estimation metric to a particular format implies the use of channel-prediction methods because the times of estimation and actual transmission are different. Channel prediction is particularly difficult in multi-path fading channels with mobiles traveling at high speeds. High speed translates into small channel coherence-time or rapid variations in channel conditions. Many researchers have addressed the prediction of channel conditions in fading channels, [34], [35], [36]. The prediction method used in this research work is presented in Chapter 6.

On the reverse link of HDR, packets of different users are transmitted at the same time in the same frequency band using code division multiple access (CDMA). The packets of the different users are separated by distinct long code

sequences, therefore the reverse link of HDR is a standard direct-sequence CDMA system that also uses soft handoff and power control to adapt to the varying conditions of the wireless fading channel.

On the forward link of HDR the sectors are transmitting at all times and at the maximum allowable power. No soft handoff or power control is in operation. Adaptive Modulation and Coding and Type II H-ARQ are used instead as mechanisms for channel adaptation. In the forward link of HDR the traffic channel is transmitted by only one sector, estimated to be the best of the sectors in the active set. The selection of this sector depends on the application, but it is usually the strongest sector as perceived by the mobile terminal.

The network layer protocol that will support the transmission of packets will likely be based on the Internet-protocol due to its widespread use. The chosen protocol for the transmission of packets is the Point-to-point protocol (PPP) [37], [38], this is a protocol used to communicate between two entities (i.e., a laptop and a host) and it is functionally below TCP/IP. PPP is the most common protocol used for modem connections today. PPP uses low overhead, methods to support differing quality of service requirements, and support of different authentication methods such as the challenge handshake authentication protocol (CHAP).

2.2.2 Forward link physical layer description

The HDR forward channel consists of the pilot channel, medium access control (MAC) channel, forward traffic channels, and control channels [31]. All the channels on the forward link are time-multiplexed in one slot, see Figure 2.3.

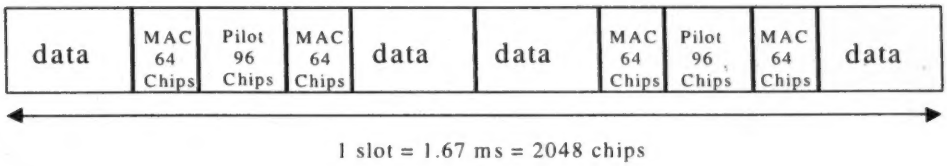

Figure 2.3. Slot structure in HDR.

The pilot channel is used for SIR estimation, selection of the best sector from the set of available sectors, and coherent demodulation. The MAC channel is sub-divided into two channels, the reverse power control channel and the reverse activity channel. The reverse power control channel transmits the power control commands to the mobile terminals, and the reverse activity channel is used to transmit MAC layer information in order to control the mobile terminals reverse channel transmissions. The forward traffic and control channels are used to convey dedicated data or control information to a mobile terminal. The forward traffic channel is a packet-based channel that provides variable data rates from 38.4kb/s to 2.4Mb/s as specified previously in Table 2.1. A simplified block diagram of the forward channel structure is depicted in Figure 2.4. The data on the traffic or control channels is first encoded using turbo codes with rates 1/3 or 1/5 [39]. The output of the encoder is scrambled and interleaved before modulation. Modulation in the forward channel can be QPSK, 8-PSK or 16-QAM [40] depending on the format chosen by the mobile terminal (see Table 2.1). The modulation symbols at the output of the modulators are de-multiplexed into 32

streams of symbols; 16 streams take the in-phase branch, and the other 16 take the quadrature-phase branch.

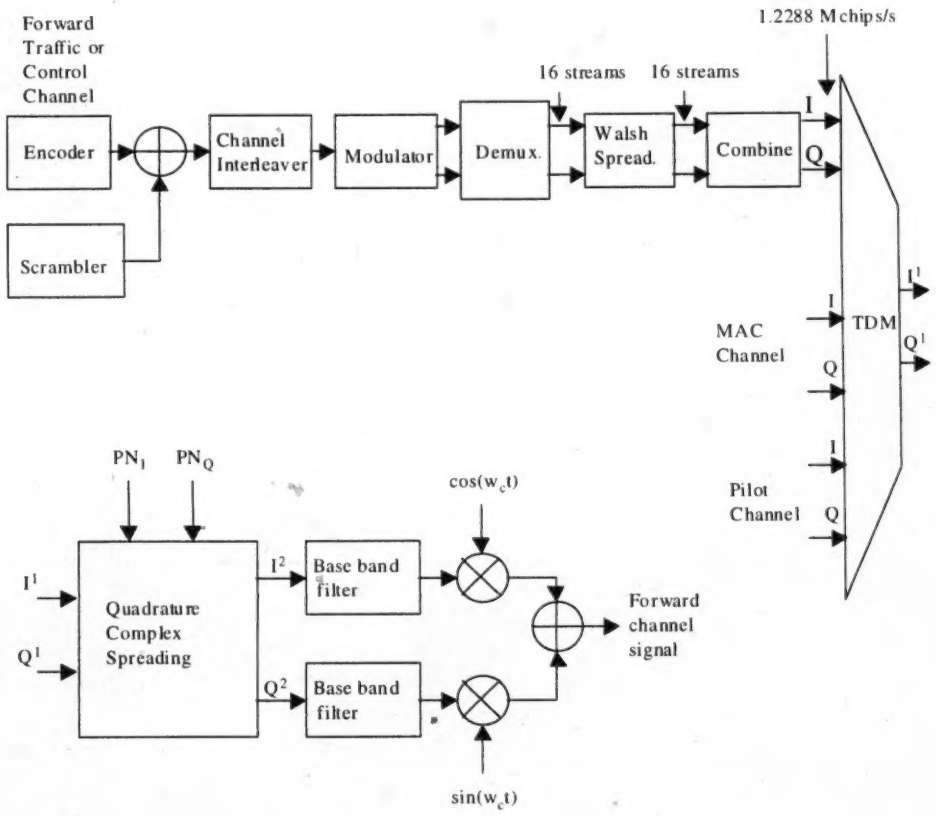

Figure 2.4. HDR forward link traffic/control channel structure.

Each stream is spread with a 16-ary Walsh function to achieve 76.8ksymbol/s, and at the next stage the 16 streams of each branch are combined to form the main stream at 1.2288 Mchips/s that is time-multiplexed with the rest of the forward channels. Symbol repetition and puncturing is performed between the modulator and de-multiplexer.

The in-phase and quadrature-phase branches at the output of the time-division multiplexer are fed into a complex spreader. The complex spreader combines the short PN sequences PN_I and PN_Q with the data in the I^1 and Q^1-phase branches according to equation (2.1).

$$I^2 = I^1 PN_I - Q^1 PN_Q$$
$$Q^2 = I^1 PN_Q + Q^1 PN_I \tag{2.1}$$

The complex spreader is performing complex multiplication. Complex spreading after Walsh spreading helps to ensure a low cross-correlation between the different channels separated by Walsh sequences. Walsh sequences have to be synchronized to be orthogonal. Due to multi-path, the synchronization of the Walsh functions is not ensured and complex spreading on top of the Walsh sequences helps to keep a low cross-correlation even in the presence a multi-path environment. The instantaneous relative powers of the in-phase and q-phase channels can differ, causing an imbalance of the transmitted signal and inefficiency of the power transmitter amplifier. Complex spreading further improves this situation by balancing the in-phase and q-phase channels. Base-band filters are used to meet bandwidth constraint requirements and minimize inter-symbol interference (ISI) [41]. In HDR the signals from sectors of different cells are identified by a particular time-shifted version of a short PN code, this can effectively reduce inter-cell interference since the cross-correlation between codes generated in this way is low.

2.2.3 Reverse link physical layer description

The reverse channel in HDR is sub-divided into the access channel and the reverse traffic channel. The access channel is further sub-divided into a pilot channel and a data channel. The traffic channel consists of the pilot channel, reverse rate indicator (RRI) channel, the data rate control (DRC) channel, the acknowledgement (ACK) channel, and the traffic channel.

The access channel is used to initiate communication with the active sector, and transmit short packets. The traffic channel is used to send user data; the rate on the reverse link varies between 9.6 kb/s to 153.6 kb/s. The RRI channel is used to indicate the rate used on the reverse traffic channel. Table 2.2 summarizes the most important parameters of the HDR system.

Bandwidth	1.25 Mhz
Chi rate	1.2288 Mchips/s
Frequency band reverse link	Cellular and PCS
Frequency band forward link	Cellular and PCS
Bit rates for data services	Forward link: 38.4 kb/s to 2.5 Mb/s Reverse link: 9.6 to 153.6 kb/s
Soft handoff	Forward link: No Reverse link: Yes
Power control	Reverse link: open loop + closed loop Forward link: Sector always transmits at maximum power.
Adaptive Modulation & Coding (AMC)	Forward link: Yes Reverse link: No
Hybrid-ARQ	Yes
Modulation	Forward link: QPSK, 8PSK, 16QAM Reverse link: BPSK
Slot length	1.67ms or 2048 chips
Error control coding	Forward link: 1/3 and 1/5 rate turbo encoder Reverse link: 1/4 and 1/2 rate turbo encoder

Table 2.2. HDR parameters.

2.2 The 1XTREME system

1XTREME represents a proposed evolution of IS-2000 that provides packet data services, and *real-time* services simultaneously in the same 1.25 MHz bandwidth. Best-effort packet data services are characterized by tolerance to delays, and low error rate requirement; examples of these services are email, and Web browsing. Real-time services are characterized by intolerance to delays, and higher tolerance to error rates than best-effort packet data services; examples of these services are voice and live video services. As in HDR, the 1XTREME system utilizes adaptive modulation and coding, hybrid ARQ, and turbo codes. Table 2.2 shows the forward link transmission formats used in 1XTREME.

Format	Modulation	Code rate
1	QPSK	½
2	QPSK	¾
3	8-PSK	½
4	8-PSK	¾
5	16-QAM	½
6	16-QAM	¾
7	64-QAM	½
8	64-QAM	¾

Table 2.3. 1XTREME forward link transmission formats [42]

The base-band 1XTREME forward traffic channel structure is depicted in Figure 2.5 [19]. Data is transmitted in frames of 5ms of time duration. The data is

transmitted in N parallel streams ($N \leq 14$), and each stream is covered with a different 16-ary Walsh function (Code Division Multiple Access). As in HDR the active sector selects the transmission format on the forward link based on SIR measurements at the mobile terminal, and the results of this measurement are sent to the active sector by the *Reverse link Quality Indicator* Channel (R-QICH) [23].

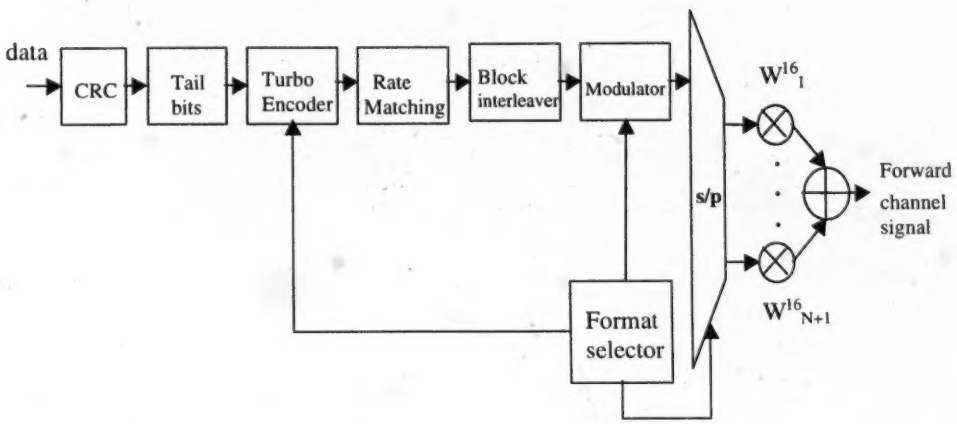

Figure 2.5. Baseband 1XTREME forward link channel structure.

2.3 Summary

The primary design fundamentals behind HDR and 1XTREME were discussed, including the Adaptive Modulation and Coding (AMC), and H-ARQ channel adaptation techniques. A brief description of the structure of the forward and reverse link channels was also presented. A more detailed description of the HDR and 1XTREME physical layers will be presented in chapter 4 under the scope of the link-level simulator description.

Chapter 3

The cellular radio system environment

3.1 Introduction

The cellular radio system environment can be characterized by its geometric structure in space and the propagation details of the wireless channel.

It is necessary to define the layout of the cells across the coverage area in order to make possible the analysis and design of cellular radio systems. In the most common geometrical model, all the cells in the coverage area are represented by non-overlapping hexagons, and the serving base station of each cell is located in the center of the hexagon. Sectors of a cell are modeled by equally dividing the area of the hexagon according to the number of sectors used. This type of cell-layout model neglects the fact that cells actually overlap causing changes in the performance of the system. In systems that utilize hard-handoff the overlapping region can cause undesired frequent switching of the mobile terminal between different base stations, and in soft-handoff systems the overlapping region will represent the most likely region for soft-handoff to occur.

The cellular radio environment modeling is also influenced by the propagation characteristics of the wireless channel. The information-bearing signals

transmitted over a wireless channel are affected by a number of adverse random propagation phenomena. These adverse phenomena represent a major limitation when high bit rate with low bit error rate transmission is desired. The cause of the wireless channel behavior is frequently attributed to path-loss, reflection, diffraction, and scattering.

Path-loss causes the attenuation of the signal as a consequence of the space separation between the transmitter and receiver antennas. The ratio of power transmitted to power received is proportional to the distance of separation. Several models have been proposed for the estimation of path-loss such as the Okumura model [43] commonly used in urban areas, the Hata model [44], and the Walfish-Ikegami model proposed by the committee 231 of the European co-operative for scientific and technical research (COST) [45].

Reflection, diffraction and scattering are related electromagnetic propagation phenomena encountered when an electromagnetic wave travels through a region with physical obstacles. All these phenomena are present in the wireless channel, and their effect is to cause multi-path fading of the transmitted signals [2].

Shadow fading is another phenomena observed in the wireless channel, it is the mean signal variation over large areas due to large obstacles such as buildings and hills; it has been characterized by a Gaussian random variable. Shadow fading takes into account the fact that different locations with the same transmitter-receiver distance have different path-loss.

Multi-path fading is the rapid fluctuation of the signal transmitted over a wireless channel. The rapid fluctuations are due to the self-interference caused by

delayed replicas of the transmitted signal that combine in the receiver antenna. When the channel bandwidth is smaller than the transmitted signal bandwidth, the delayed replicas arrive at the receiver with large differences in time, causing inter-symbol interference (ISI) and frequency selective fading. When the signal bandwidth is smaller than the channel bandwidth the signal undergoes what is called flat fading [2], [46]. In a CDMA system the RAKE receiver helps to resolve the different paths when the multi-path fading is frequency-selective. Other types of multi-path fading are fast and slow multi-path fading. In fast fading the channel-variation times are faster than the symbol period, in this type of channel there is a high frequency spread caused by the high Doppler shift of the frequencies. High Doppler shift is caused by high mobile speed. Slow fading is characterized by channel-variation times larger than the symbol period.

This chapter presents the cellular radio environment models and assumptions taken in this research work. Section 3.2 describes the cellular layout used. Section 3.3 presents the path-loss Walfish-Ikegami model, the cell size computation, and the shadow-fading model used, and finally section 3.4 addresses the multi-path fading model.

3.2 Cellular geometric structure

The cell layout is depicted in Figure 3.1, as given in [22]. There are 19 cells consisting of two rings of 3 sectors each. There are 57 sectors altogether.

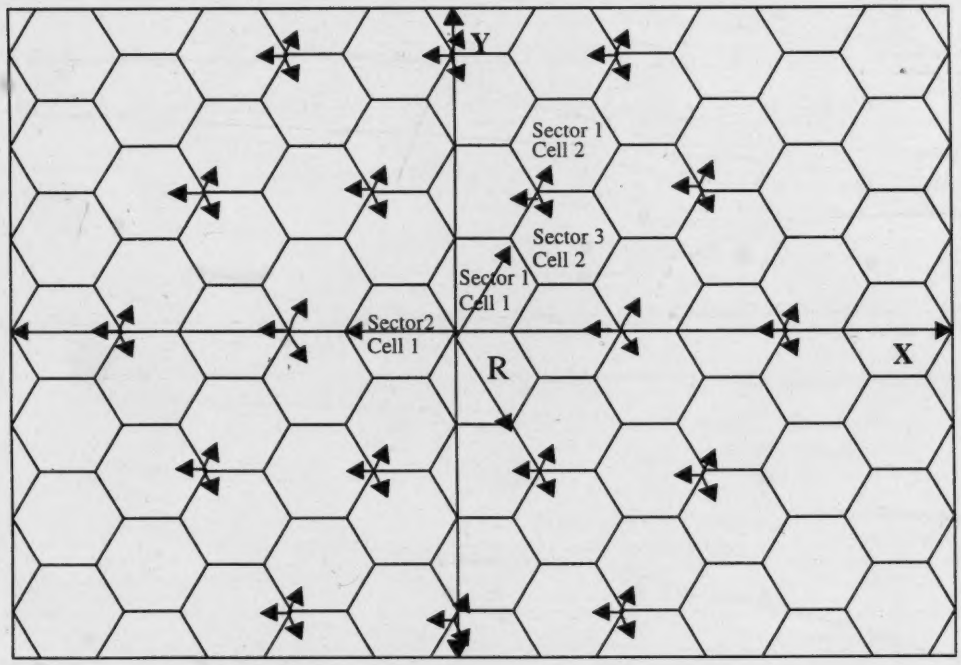

Figure 3.1. Cell layout as recommended in [6]. Bore-sight of antennas is shown with small arrows at the center of 3 sectored cells.

3.3 Path-loss and shadow fading models

The path-loss in free-space, assuming an isotropic antenna is given by Equation 3.1 [2]

$$L_{fs} = \left(\frac{4\pi d f_c}{c}\right)^2 \tag{3.1}$$

d = distance separation between the transmitter and receiver antennas;

c = speed of light; f_c = frequency of the transmitted sinusoid waveform in Hz.

The free-space path-loss formula is used in the design of line-of-sight (LOS) communication systems where there is an unobstructed path between the transmitter and receiver antennas; an example of such a system is the microwave-radio-link communication system. The cellular radio system environment rarely presents LOS radio links. More accurate models have to be used to estimate the path-loss attenuation in cellular radio environments. A commonly used path-loss estimation formula is given by Equation 3.2 [2]

$$L = \overline{L}_r(d_0)\left(\frac{d}{d_0}\right)^n \tag{3.2}$$

In equation 3.2, d_0 represents a reference distance taken close to the transmitter antenna, $\overline{L}_r(d_0)$ is the average measured path-loss at reference-distance d_0, and n is a exponent that indicates the degree of attenuation suffered by a signal depending on distance separation; n ranges between 3.0 to 5.0 [10]. The exponent n depends on the structure of the physical surroundings. The model in equation (3.2) is known as the general empirical model for the estimation of path-loss.

In this research work the COST231-Walfish Ikegami model is used [45], [47]. The Walfish-Ikegami model is applicable for transmitter-receiver distances greater than or equal to 20 meters, and base-station antennas above or below the roof tops. For non-line-of-sight (NLOS) propagation the Walfish-Ikegami model is given by

$$L = L_{bf} + L_{rts} + L_{msd} \tag{3.3}$$

where

$$L_{bf} = 32.4 + 20\log(d) + 20\log(f_C); \tag{3.4}$$

$$L_{rts} = -16.9 - 10\log(w) + 10\log(f_C) + 20\log(H - h_m) + L_{ori.}); \tag{3.5}$$

$$L_{msd} = 54 - 18\log(1 + h_b - H) + 18\log(d) + \left[-4 + 0.7\left(\frac{f_C}{925} - 1\right)\right]\log(f_C) - 9\log(b). \tag{3.6}$$

are free space, roof-top-to-street diffraction, and multi-screen diffraction losses respectively; The path-loss in equations (3.3)-(3.6) is expressed as a function of the separation distance between transmitter and receiver antennas (d), the carrier frequency in MHz (fc), the street width (w), building separation (b), base-station and mobile station antenna heights (h_b, h_m), average rooftop height (H). L_{ori} is the orientation loss. We have assumed $L_{\text{ori}} = 0\,\text{dB}$, which is a usual default value.

Cell size calculation is performed using the Walfish-Ikegami model and values presented in Table 3.1. The path loss is computed along the bore sight line of the antenna. After inserting the parameters given by Table 3.2 in equations (3-3)-(3-6), and given $L_{b(\max)} = 130.87\,\text{dB}$; the cell radius is computed to be 473 meters, which implies site-to-site separation of 709 m.

The directivity loss (horizontal pattern) of the antenna (EMS, RR65-18-00DP) used is available as a data file. The directivity loss vs. relative orientation with respect to the antenna bore sight can be seen in Figure 3.2, The 3dB bandwidth is

$\theta_{3dB} \cong 66^0$,and the front-to-back ratio for this antenna is about 35 dB. This ratio affects the maximum available SIR in each sector.

Parameter	Value	Comments
(a) Transmission Power per sector Pt_{max}.	42.3 dBm (17 W)	-
(b) BS Bore-sight antenna gain, G_b.	17.54 dBi	Antenna EMS WIRELESS RR 65-18-00DP
(c) Antenna cable Loss, L_c.	3 dB	-
(d) Effective data transmission power	80% of Pt_{max}	-
(e) Total transmitted power on the traffic channel at the bore sight of the antenna.	a+b-c+d=55.87 dBm	-
(f) Penetration loss, L_p.	10.0 dB	-
(g) Minimum required received data channel power on BS antenna bore sight line, P_{rec}.	-85 dBm	Includes large scale fading margin
(h) PSD of thermal noise	-174 dBm/Hz	Ignored
(j) Maximum allowable over-the-air loss, $L_{b(max)}$.	e-f-g=130.87 dB	-

Table 3.1. Link budget values for the forward Link

Parameter	Range	Values Used in Simulation
Carrier frequency	$800 \le f \le 2000$ MHz	1960 MHz
Distance to BS antenna	$0.02 \le d \le 5$ km	Variable
BS antenna height	$4 \le h_b \le 50$ m	3 m above average roof top
MS antenna height	$1 \le h_m \le 3$ m	1.5 m
Building separation *b*	-	40 m
Street width *w*	-	20 m
Average roof top height H	-	18 m

Table 3.2. Values of parameters used in cell size computation.

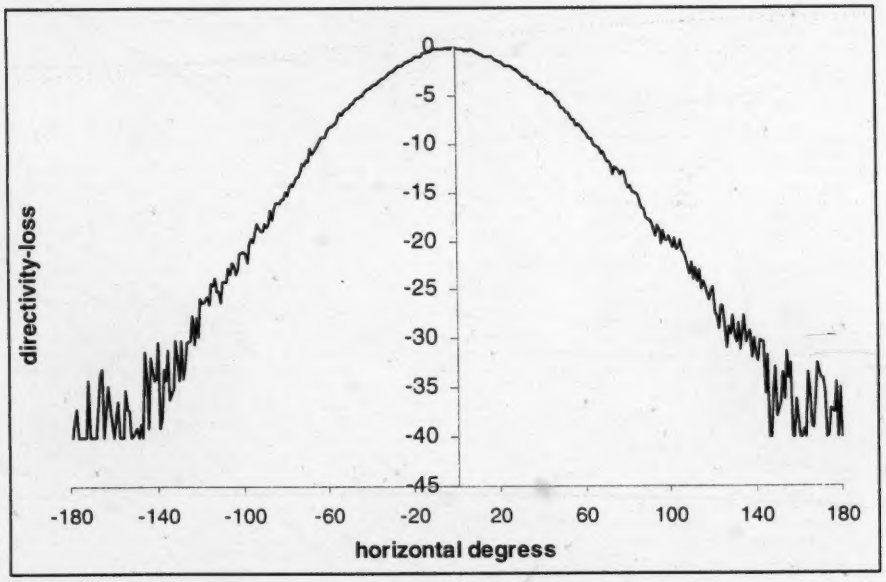

Figure 3.2. The directivity loss pattern for the EMS RR65-18-00DP antenna.

The log-normal shadowing effect is modeled by a zero mean Gaussian random process added to the path-loss in dB [47]. Therefore, the signal power averaged over small scale is given by

$$P^i{}_{\text{rec}} = P_{\text{t}} + G_{\text{b}} + G^i{}_{\text{d}}(\theta) - L_{\text{p}} - L^i{}_{\text{b(dB)}} - \text{X}^i, \qquad i = 1,\Lambda\ ,57. \tag{3.7}$$

where, $P^i{}_{\text{rec}}$ is the received power by a mobile terminal from sector i, P_t is the transmitted power, G_b is the base station antenna gain, $G^i{}_{\text{d}}(\theta)$ is the directivity loss, L_{p} is penetration loss, $L^i{}_b$ is given by (3.3), L^i is the path-loss between a mobile terminal and sector i, and X^i is the shadowing variable.

On the dB scale, X^i is a zero mean Gaussian random variable with standard deviation σ_X. A typical range of values for σ_X in macro-cellular environments is 5-12 dB. In micro-cellular environments, a typical value of σ_X is 4-13 dB [47]. We use 6.5 dB in our simulations.

The cross-correlation of the log-normal shadowing term for signals arriving from base stations i and j is denoted by α.

$$\frac{E[X^i X^j]}{\sqrt{Var(X^i)}\sqrt{Var(X^j)}} \equiv \alpha, \qquad i \neq j,\ i = 1,\Lambda\ ,19,\ j = 1,\Lambda\ ,19. \tag{3.8}$$

In this work we assume a constant value of $\alpha = 0.5$ for shadowing cross-correlation of signals received from different cell sites. The cross-correlation of shadowing variables between signals from different sectors of the same base station is one [47]. To ensure proper cross-correlation of the log-normal shadowing variable, X^i is generated as a linear combination of a component representing the base-station dependent shadowing Z^i such that $E[Z^i Z^j] = 0$ for $i \neq j$, and a component Z common to all base stations. In order to generate cross-correlated Gaussian sequences, the shadowing variable can be written as

$$X^i = aZ + bZ^i,\ i = 1,2,\ldots,19;\ a \geq 0,\quad b \geq 0. \tag{3.9}$$

where Z, Z^i are i.i.d Gaussian random variables with zero mean and standard deviation $\sigma_Z = \sigma_X$.

Note that

$$\sigma_X{}^2 = E[X^{i2}] = a^2 E[Z^2] + b^2 E[Z^{i2}] = (a^2 + b^2)\sigma_Z{}^2,$$

Therefore, $(a^2 + b^2) = 1$ (3.10)

From (3.8) - (3.10)

$$E[X^i X^j] = \alpha\sigma_X{}^2 = a^2 E[Z^2],$$

Therefore, $a^2 = \alpha$, $b^2 = 1 - \alpha$. (3.11)

By taking $a = b = \sqrt{1/2}$ in Equation (3.9) we can generate Gaussian random sequences with 50% cross-correlation and standard deviation σ_X.

Shadow fading is spatially auto-correlated (i.e., values of shadow fading terms are correlated in different points in space). Spatial auto-correlation of shadow fading has to be taken into account when the mobile is moving. In this research work the spatial auto-correlation is modeled as an exponential function as proposed by Gudmundson in [48].

$$\Phi(k) = E[X^i{}_d X^i{}_{d+k\Delta d}] = (\sigma_X)^2 \; e^{-\frac{|k|\Delta d \ln 2}{d_{dec}}} = (\sigma_X)^2 \; e^{-\frac{|k|\Delta v \ln 2}{d_{dec}}} \quad (3.12)$$

where d_{dec} is the decorrelation distance, and v is the mobile speed. In [20], and [22] $d_{dec} = 20\,\text{m}$ is suggested for vehicular test environments, and $d_{dec} = 5\,\text{m}$ for

outdoor to indoor and pedestrian environments. In our simulations, we use these two values for vehicular B and pedestrian A environments, respectively. The vehicular B and pedestrian A radio environment specifications and definitions are given in [20]. A vehicular B environment is characterized by larger cells, higher transmit powers and higher mobile speeds; the pedestrian A environment main characteristics are small cell size and low mobility.

The update rate of the shadowing factor should in principle depend on the mobile velocity and the relative contribution of shadowing to $L^i_{b(\mathrm{dB})} + \mathrm{X}^i$. We have decided to update the shadowing variable at $\Delta d = d_{\mathrm{dec}}/10$ intervals.

The exponential auto-correlation function given by (3-12) can be generated with a first order discrete time recursive filter [47];

$$X^i{}_{k+1} = \xi X^i{}_k + (1-\xi)\upsilon_k\,; \tag{3.13}$$

where X_{k+1} is the updated shadow term at position k+1 that is correlated with the previous value X_k at position k. ξ is a parameter used to control the spatial auto-correlation of shadowing, and υ_k is a zero-mean Gaussian random variable with standard deviation σ_υ. The auto-correlation of (3.13) is given by

$$\Phi(n) = E[\mathrm{X}^i{}_k \mathrm{X}^i{}_{k+n}] = \frac{1-\xi}{1+\xi}\sigma_\upsilon{}^2 \xi^{|n|}. \tag{3.14}$$

Comparing equation (3.12) and (3.14), it is possible to find a value of ξ and σ_v to make the auto-correlation of the recursion in (3.13) equal to that in (3.12). Choosing

$$\xi = e^{-\frac{\Delta d \ln 2}{d_{dec}}} \text{ ; and } \sigma_v{}^2 = \frac{1+\xi}{1-\xi}\sigma_X{}^2. \tag{3.15}$$

The auto-correlation of the discrete recursion in equation (3.13) becomes

$$\Phi(n) = (\sigma_X{}^2)e^{-\frac{|n|\Delta d \ln 2}{d_{dec}}}. \tag{3.16}$$

Therefore the recursion in (3.13) can be used with the values in (3.15) to generate a sequence of correlated Gaussian random numbers; each number $X_k{}^i$ is associated with the position $k\Delta d$.

In order to model shadow fading for our simulation we are interested in 19 sequences of Gaussian random numbers with fix cross-correlation of 50%, auto-correlation given by equation (3.16), and with standard deviation σ_X. In order to achieve the above constrains the following procedure is applied.

We first generate 19 sequences with cross-correlation of 50% as follows

$$v^i = \sqrt{\frac{1}{2}}Z + \sqrt{\frac{1}{2}}Z^i \quad i = 1,2,\ldots,19; \tag{3.17}$$

where

$$Z = Gaussian\left(0\,\text{mean}, {\sigma_Z}^2\right)$$
$$Z^i = Gaussian\left(0\,\text{mean}, {\sigma_Z}^2\right)$$
$${\sigma_Z}^2 = {\sigma_v}^2 = \frac{1+\xi}{1-\xi}\left({\sigma_X}^2\right)$$
$$\xi = e^{-\frac{\Delta d \ln 2}{d_{dec}}}$$

The sequences in (3.17) are used next to generate the 19 sequences with desired auto-correlation and fixed cross-correlation of 50% as follows

$$X^i{}_{k+1} = \xi X^i{}_k + (1-\xi)v_k{}^i \quad i = 1,2,\ldots,19; \quad 0 \le k < N; \tag{3.18}$$

where N is the desired length of the sequences. Figure 3.3 shows the comparison between an ideal auto-correlation function and the auto-correlation of 200,000 shadow numbers generated using equations (3.17) and (3.18). $\sigma_X = 6.5\,\text{dB}$ and $d_{dec} = 5\text{ m}$ ($\Delta d = 0.5\,\text{m}$) are assumed.

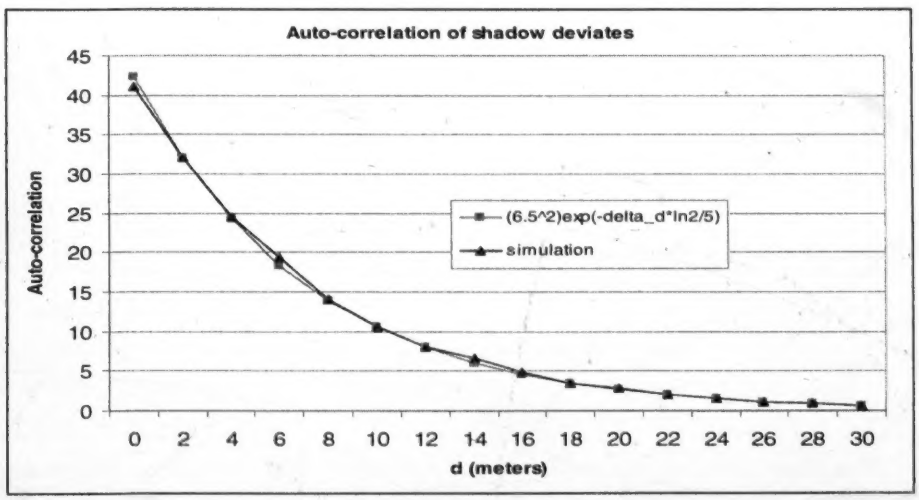

Figure 3.3. Ideal and simulated auto-correlation of 200,000 log-normal shadow fading variables.

3.4 Multi-path fading model

To take into account the impact of fast fading of the signal on the performance of the systems, Rayleigh fading is modeled. In a Rayleigh fading channel, the probability density function (pdf) of the received signal power γ is given by the exponential distribution

$$p_\gamma(\gamma) = \frac{1}{\bar{\gamma}} e^{-\gamma/(\bar{\gamma})} \tag{3.19}$$

where $\bar{\gamma} = 10^{P_{rec}/10}$ is the small scale averaged signal power. P_{rec} (dBm) is given by (3.7). In the simulation, an exponential random variable with mean P_{rec} is obtained by multiplying P_{rec} by the normalized exponential random variable γ with $\bar{\gamma} = 1$. Alternatively, (3.7) is replaced by

$$P^i{}_{rec} = P_t + G_b + G^i{}_d(\theta) - L_p - L^i{}_{b(dB)} - X^i + \gamma_{(dB)}, \qquad i = 1, \Lambda, 57, \tag{3.20}$$

where $p_\gamma(\gamma) = e^{-\gamma}$.

The Rayleigh fading process exhibits an auto-correlation that can be described using Clark's model [49]. In Clark's model, the field incident on the mobile antenna is assumed to be comprised of N azimuthal plane waves with arbitrary carrier phases, arbitrary azimuthal angles of arrival, and equal average amplitudes. The equal average amplitude assumption is based on the fact that in the absence of a direct line of sight path, the scattered components arriving at a

receiver from all directions will experience similar attenuation over small distances. In this model, the auto-correlation function of the real and imaginary parts $x_R(t)$ and $x_I(t)$ of the complex envelope is given by [47]

$$\phi_{x_R x_R}(\tau) = \phi_{x_I x_I}(\tau) = \Omega_P J_0(2\pi f_{D\max}\tau), \tag{3.21}$$

where J_0 is the zero-order Bessel function of the first kind, Ω_P is the total average received power from all multi-path components, and $f_{D\max}$ is the maximum Doppler frequency. The power spectral density (psd) of $x_R(t)$ and $x_I(t)$ is given by [47]

If $\Omega_p = E[r^2(t)]/2$, then

$$S_{x_R x_R}(f) = S_{x_I x_I}(f) = \begin{cases} \dfrac{\Omega_P}{2\pi f_{D\max}} \dfrac{1}{\sqrt{1-(f/f_{D\max})^2}} & |f| \le f_{D\max}, \\ 0 & \text{otherwise.} \end{cases} \tag{3.22}$$

Where *r(t)* is the received band-pass signal. It should be noted that the psd of the real and imaginary parts of the amplitude of the base band signal is singular at $f = \pm f_{D\max}$. A modified Smith method [50] is used to generate a Rayleigh random process with the auto-correlation that approximates (3.22). In this method, first, *N* samples of a complex Gaussian white noise in frequency domain are filtered to obtain psd given by (3-22). Then IDFFT is used to obtain a sequence of *N* correlated complex Gaussian random variables in the time domain.

A block diagram of the modified Smith method is given in Figure 3.4. Since psd of a discrete time process is periodic with period equal to f_{sampling}, instead of sampling a Gaussian white noise in frequency domain in $|f| \le f_{D\max}$ as (3-22) suggests, one can sample the Gaussian noise in $0 \le f \le f_{D\max}$ and $f_{\text{sampling}} - f_{D\max} \le f \le f_{\text{sampling}}$ intervals. More specifically, in this method, a white Gaussian noise in frequency domain is passed through a low-pass filter with filter coefficients given in (3-23).

$$F_M[k] = \begin{cases} 0 \quad k = 0, \\ \sqrt{\dfrac{1}{2\sqrt{1-\left(\dfrac{k}{Nf_m}\right)^2}}} \quad k = 1,2,\mathrm{K}\ ,k_m - 1, \\ \sqrt{k_m\left[\dfrac{\pi}{2} - \arctan\left(\dfrac{k_m - 1}{\sqrt{2k_m - 1}}\right)\right]} \quad k = k_m, \\ 0 \quad k = k_m + 1,\mathrm{K}\ ,N - k_m - 1, \\ \sqrt{k_m\left[\dfrac{\pi}{2} - \arctan\left(\dfrac{k_m - 1}{\sqrt{2k_m - 1}}\right)\right]} \quad k = N - k_m, \\ \sqrt{\dfrac{1}{2\sqrt{1-\left(\dfrac{N-k}{Nf_m}\right)^2}}} \quad k = N - k_m + 1,\mathrm{K}\ ,N-1 \end{cases} \tag{3.23}$$

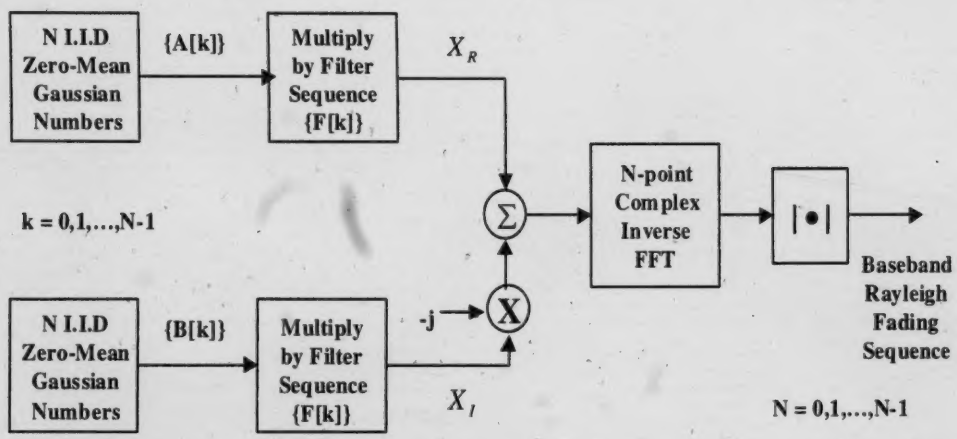

Figure 3.4. Block diagram of the modified Smith method.

In (3-23), $f_m = f_{D\max} / f_{\text{sampling}}$ is the ratio of the maximum Doppler frequency to sampling frequency and $k_m = \lfloor f_m N \rfloor$, where N is the number of sampling points in the frequency domain and the corresponding number of points per period of the auto-correlation function. After filtering the sampled white Gaussian noise in frequency domain, the inverse discrete Fourier transform (IDFT) is used to obtain the complex fading random process in the time domain. The filter coefficients are chosen in such a way that the real and imaginary parts of the output variables are statistically independent. The modified Smith model presented has the advantage of less computational complexity in comparison with the standard Smith model. In the standard Smith model [2] two branches similar to the one in Figure 3.4 are used to produce the desired result due to the independence requirement of the real and imaginary parts of the Gaussian sequences after IDFT operation.

The normalized real and imaginary parts of the output of the IDFT are

$$x_c(n) = x_R(n) + jx_I(n) \tag{3.24}$$

where n refers to sampling time t_n. The auto-correlation is given by

$$\phi_{x_R x_R}(\tau) = \phi_{x_I x_I}(\tau) = J_0(2\pi f_{D\max}\tau). \tag{3.25}$$

where τ can take discrete values only.

Simulated and theoretical pdf's of Rayleigh variables generated using the modified-Smith method presented above are shown in Figure 3.5. In this figure the comparison is made with the normalized pdf function for which $2\sigma^2 = \Omega_P = 1$. Figures 3.6 and 3.7 show a comparison of the theoretical and simulated auto-correlation of x_R for user speeds of 3 and 60km/h. At these speeds the Doppler frequency is 5.3 and 105.6Hz respectively. As can be seen by the auto-correlation functions, when higher speeds are involved, the correlation of Rayleigh fading numbers decreases faster in time

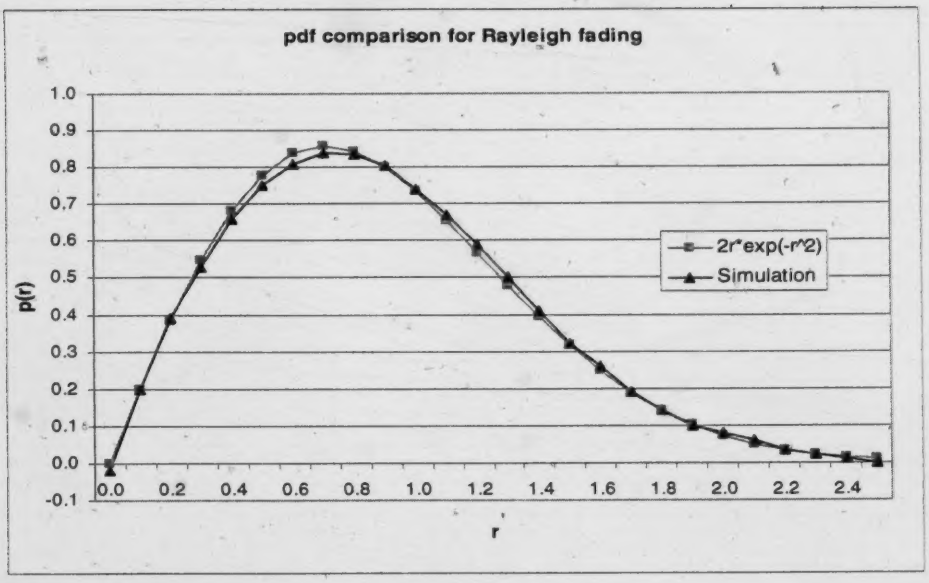

Figure 3.5. pdf comparison of theoretical and simulated correlated Rayleigh process.

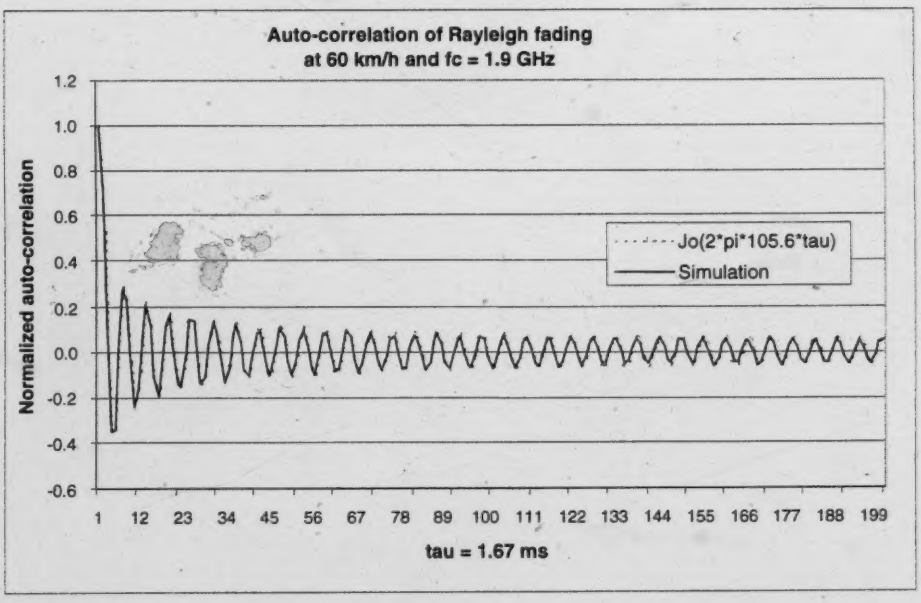

Figure 3.6. Auto-correlation comparison of theoretical and simulated Rayleigh process at 60km/h with f_c = 1.9GHz.

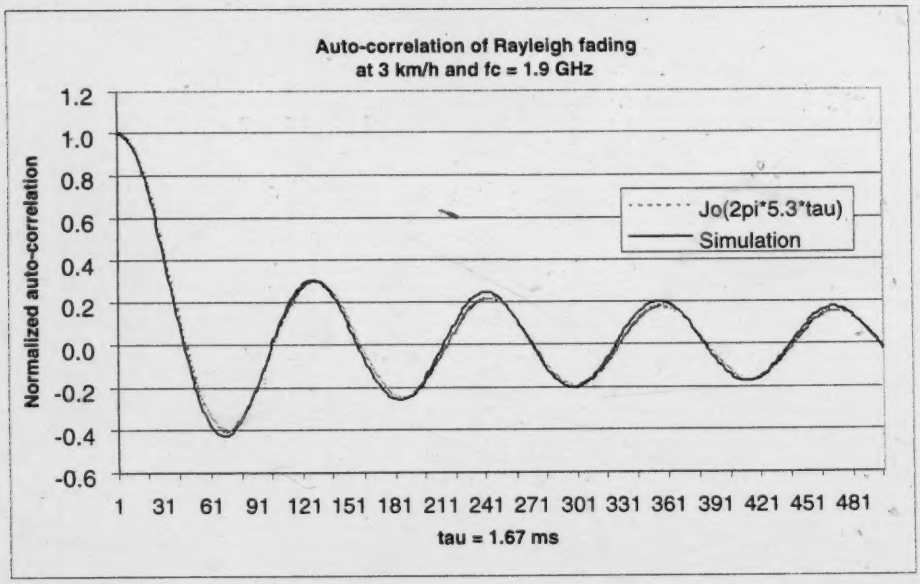

Figure 3.7. Auto-correlation comparison of theoretical and simulated Rayleigh process at 3km/h with f_c = 1.9GHz.

3.5 Summary

We have presented the algorithms and equations to model the cellular radio environment for this research work. The cell layout defined in [22] is going to be used for vehicular B and pedestrian A radio environments as defined in [20]. The COST-231 Walfish-Ikegami model will be implemented for path-loss estimation. Shadow fading will be modeled as a log-normal process with fix cross-correlation to model shadow fading coming from different cell-sites and exponential auto-correlation as proposed in [48] to model spatial correlation. The method proposed in [50] will be used to model multi-path fading at different speeds.

Chapter 4

Simulation structure and link level simulations

4.1 Introduction

There are two possible approaches for the simulation of a cellular radio system. In one approach the system is simulated entirely from the transmitter-receiver modeling of a single radio link to the modeling of radio-links and operations for a multitude of mobiles and base stations present in the network. This approach is the most accurate one, but its complexity is extremely high considering the number of waveforms to generate and the simulation run-time. A preferred two-stage method is to separate the simulation of the transmitter-receiver pair from the simulation of the operations and signals of the entire system.

In the two-stage approach, the simulation of the transmitter-receiver pair is called the link-level simulation, and the entire-network simulation is called the system-level simulation. The link and system level simulations have to be properly interfaced to obtain the desired network performance results.

Section 4.2 describes the general simulation structure applied in this research work and the interface between the link-level and system-level simulations.

Section 4.3 presents the link-level simulation structure and results for HDR and 1XTREME; in this section a more detailed description of the physical layer of HDR and 1XTREME will be presented. System-level simulation will be described in Chapter 5.

4.2 General simulation structure

The combined link-level and system-level simulations represent the modeling of the entire cellular system. First the link-level simulations are performed independently and the results are fed into the system-level simulator. A block diagram description of this operation is shown in Figure 4.1. The link-level simulation section comprises a link level simulator that models the transmitter-

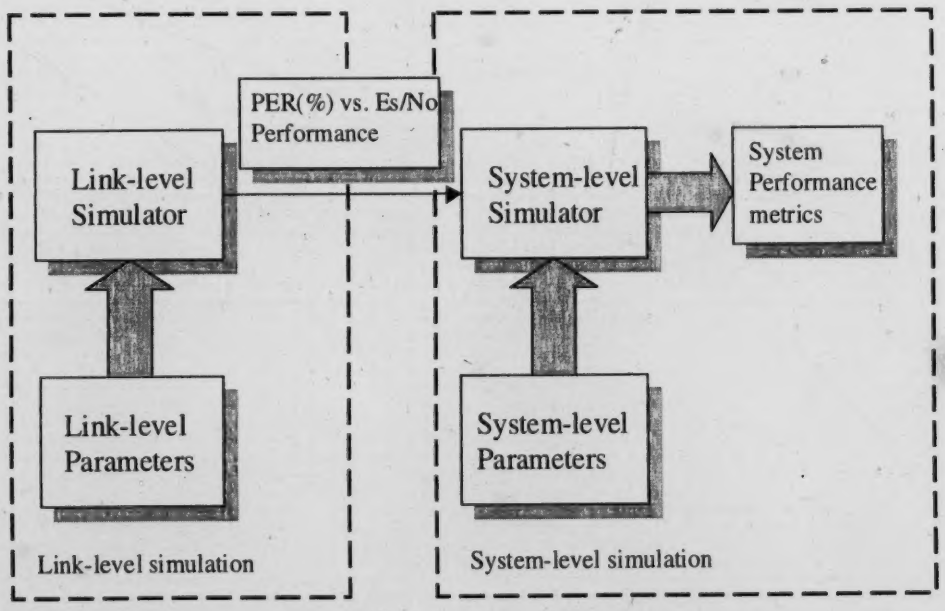

Figure 4.1. General simulation structure of HDR and 1XTREME.

-receiver structure with a time resolution of a modulation symbol; the encoder/decoder, modulator/demodulator and signal processing associated with

the operations of a single transmitter-receiver pair are modeled. The link-level simulator also includes the model and assumptions of the channel between the transmitter and receiver. For this research work the channel used in the link level simulator is an Additive White Gaussian Noise (AWGN) channel. The reason for this choice is that HDR and 1XTREME are systems designed for bursty packet transmission within short-time slots (1.67ms for HDR, and 5ms for 1XTREME) during which the fading radio channel is practically time-invariant, even for highly mobile user terminals (up to 60km/h). Hence, the SIR seen by the mobile receiver over one slot is practically constant and AWGN results are applicable. At 60km/h and carrier frequency of 2GHz the coherence time of the radio channel [2] is on the order of 5ms. Hence, the radio channel will display some variability over one 1XTREME slot. This variability is accounted for in system level simulations. It also needs to be mentioned that HDR and 1XTREME systems are primarily designed for nomadic users as pointed out in Chapter 1. Nomadic users can be stationary for the duration of a given transmission session.

The parameters of the link-level simulator are the different formats of transmission, the modulations used, the packet sizes, the code rates, interleaver method etc. The desired output of the link-level simulator is the packet error rate (PER) for every format of transmission in the AWGN channel for different fixed values of energy-symbol over noise ratio (E_s / N_o). The AWGN curves of PER (%) vs. E_s / N_o out of the link-level simulator are fed into the system-level simulator for its operation. The system level simulation will be described in Chapter 5.

4.3 Link level simulations

4.3.1 Structure and functionality of the HDR and 1XTREME forward links.

4.3.1.1 HDR forward traffic channel transmission formats

The HDR Forward Traffic Channel is a packet-based, variable-rate channel. The user data for an access terminal is transmitted at a data rate that varies from 38.4kbp/s to 2.4576Mbp/s. The data is encoded in blocks called physical layer packets. The physical layer packets and rates supported by the HDR Forward Traffic Channel are specified in Table 4.1, along with the corresponding modulation/coding schemes (MCS) and maximum allowed number of re-transmissions. Table 4.1 includes also bit rates resulting from early termination of retransmissions, occurring when a positive acknowledgement is sent by a mobile before the maximum allowed number of retransmissions is reached. Link-level simulations have generated AWGN PER vs. E_s / N_o curves for all rates listed in this table.

Transmission Format Number	Max. Allowed Slots	Transmitted Slots	Packet Size (bits)	Preamble Size (chips)	Data Rate (kbp/s)	Turbo Code Rate	Modul.
1	16	16	1,024	1,024	38.4	1/5	QPSK
2	16	15	1,024	1,024	40.96	1/5	QPSK
3	16	14	1,024	1,024	43.89	1/5	QPSK
4	16	13	1,024	1,024	47.26	1/5	QPSK
5	16	12	1,024	1,024	51.2	1/5	QPSK
6	16	11	1,024	1,024	55.85	1/5	QPSK
7	16	10	1,024	1,024	61.44	1/5	QPSK
8	16	9	1,024	1,024	68.27	1/5	QPSK
9	16	8	1,024	1,024	76.8	1/5	QPSK
10	16	7	1,024	1,024	87.77	1/5	QPSK
11	16	6	1,024	1,024	102.4	1/5	QPSK
12	16	5	1,024	1,024	122.88	1/5	QPSK
13	16	4	1,024	1,024	153.6	1/5	QPSK
14	16	3	1,024	1,024	204.8	1/5	QPSK
15	16	2	1,024	1,024	307.2	1/5	QPSK
16	16	1	1,024	1,024	614.4	1/5	QPSK
17	8	8	1,024	512	76.8	1/5	QPSK
18	8	7	1,024	512	87.77	1/5	QPSK
19	8	6	1,024	512	102.4	1/5	QPSK
20	8	5	1,024	512	122.88	1/5	QPSK
21	8	4	1,024	512	153.6	1/5	QPSK
22	8	3	1,024	512	204.8	1/5	QPSK
23	8	2	1,024	512	307.2	1/5	QPSK
24	8	1	1,024	512	614.4	1/5	QPSK
25	4	4	1,024	256	153.6	1/5	QPSK
26	4	3	1,024	256	204.8	1/5	QPSK
27	4	2	1,024	256	307.2	1/5	QPSK
28	4	1	1,024	256	614.4	1/5	QPSK
29	2	2	1,024	128	307.2	1/5	QPSK
30	2	1	1,024	128	614.4	1/5	QPSK
31	1	1	1,024	64	614.4	1/5	QPSK
32	4	4	2,048	128	307.2	1/3	QPSK
33	4	3	2,048	128	409.6	1/3	QPSK
34	4	2	2,048	128	614.4	1/3	QPSK
35	4	1	2,048	128	1,228.8	1/3	QPSK
36	2	2	2,048	64	614.4	1/3	QPSK
37	1	1	2,048	64	1,228.8	1/3	QPSK
38	2	2	3,072	64	921.6	1/3	8PSK
39	1	1	3,072	64	1,843.2	1/3	8PSK
40	2	2	4,096	64	1,228.8	1/3	16QAM
41	1	1	4,096	64	2,457.6	1/3	16QAM

Table 4.1. Physical layer packet sizes and rates supported by the HDR Forward Channel.

4.3.1.2 1XTREME forward shared channel transmission formats

The Forward Shared Channel (F-SHCH) is one of the two new channels on the forward link of cdma2000 introduced in the 1XTREME system. The 1XTREME Forward Shared Channel uses an adaptive modulation and coding scheme (MCS) with four possible types of modulation: QPSK, 8PSK, 16QAM and 64QAM. The packet lengths and rates supported by the Forward Shared Channel are specified in Table 4.2. The Forward Shared Channel can be mapped to multiple (*N* up to a maximum of 14 codes) parallel code channels of Walsh length 16.

Transmission Format Number	Packet Size (Bits)	Data Rate (kbps)	Turbo Code Rate	Modulation Scheme
1	384 x *N*	76.8 x *N*	½	QPSK
2	576 x *N*	115.4 x *N*	¾	QPSK
3	768 x *N*	153.6 x *N*	½	16QAM
4	864 x *N*	172.8 x *N*	¾	8PSK
5	1152 x *N*	230.4 x *N*	¾	16QAM
6	1728 x *N*	345.6 x *N*	¾	64QAM

Table 4.2. Physical layer packet sizes and rates supported by the 1XTREME Forward Shared Channel (N is the number of orthogonal codes allocated to the Forward Shared Channel)

4.3.1.3 Turbo encoder and decoder

The HDR Forward Traffic Channel physical layer packets (excluding the 6-bit TAIL field) and 1XTREME Forward Shared Channel packets (including two reserved bits) are encoded with a turbo encoder of code rate *R* (see Tables 4.1 and 4.2). The turbo encoder will add an internally generated tail of 6/*R* output code symbols, so that if the number of input bits to the turbo encoder is N_{turbo}, the

turbo encoder generates N_{turbo}/R encoded data output symbols followed by $6/R$ tail output symbols.

4.3.1.3.1 Turbo encoder

The HDR Forward Traffic Channel and the 1XTREME Forward Shared Channel use the same turbo encoder, as shown in Figure 4.2. It employs two systematic recursive convolutional (RSC) encoders [51], [39], connected in parallel, with a turbo interleaver preceding the second convolutional encoder. The recursive convolutional codes are the constituent codes of the turbo code. They have the same transfer function given by

$$G(D)=\left[1 \quad \frac{n_0(D)}{d(D)} \quad \frac{n_1(D)}{d(D)}\right] \tag{4.1}$$

where $d(D)=1+D^2+D^3$, $n_0(D)=1+D+D^3$, and $n_1(D)=1+D+D^2+D^3$.

Initially, the states of the constituent encoder registers in Figure 4.2 are set to zero. Then, the constituent encoders are clocked with the two switches in the upper positions. The encoded data output symbols are generated by clocking the constituent encoder N_{turbo} times with the switches in the upper positions.

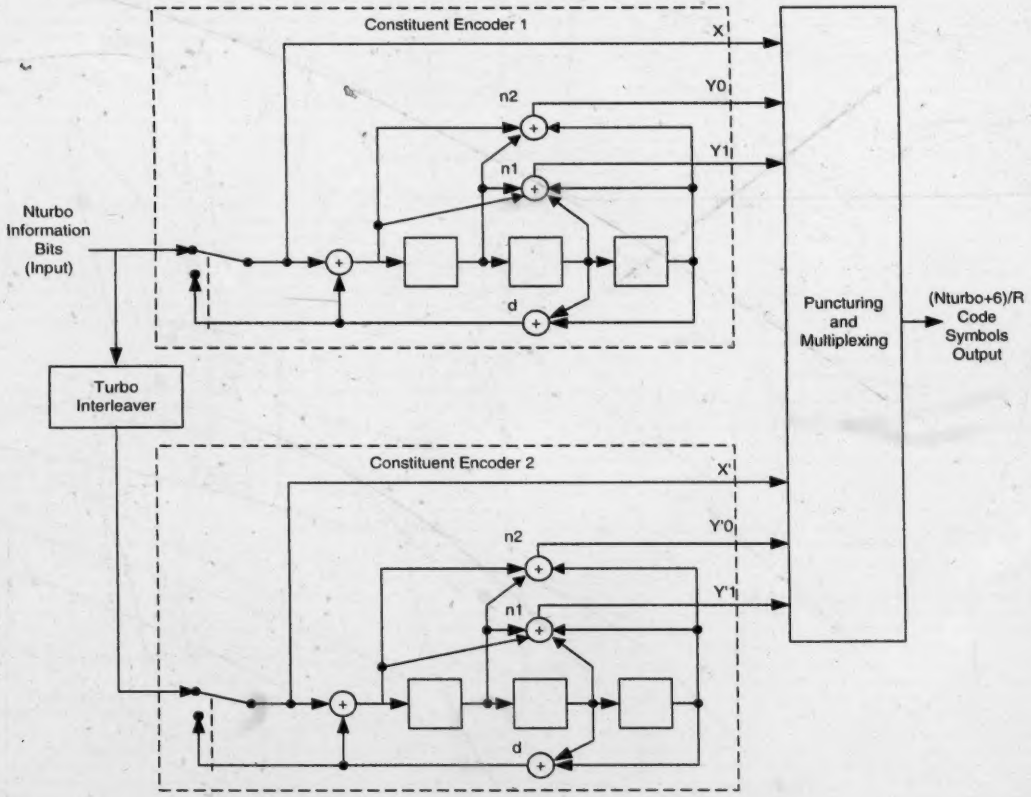

Figure 4.2. Turbo encoder used in HDR and 1XTREME.

The resulting constituent encoder output sequences are then punctured as specified in Table 4.3. Within a puncturing pattern, a '0' means that the symbol shall be deleted and a '1' means that the symbol shall be passed.

	Code Rate *R*			
Output	¾	1/2	1/3	1/5
X	111111	11	1	1
Y_0	100000	10	1	1
Y_1	000000	00	0	1
X'	000000	00	0	0
Y'_0	000100	01	1	1
Y'_1	000000	00	0	1

Table 4.3. Puncturing pattern for the data bit periods. The table is read first from top to bottom and then from left to right. (e.g., for code rate ¾, 8 coded symbols are passed out of 6 data symbols)

The turbo encoder shall generate $6/R$ tail output symbols following the encoded data output symbols. The tail output symbols are generated by clocking each constituent encoder separately three times with the switch in the lower position. The resulting constituent encoder output symbols are then punctured and repeated as specified in Table 4.4.

	Code Rate *R*			
Output	¾	½	1/3	1/5
X	111000	111000	111000	111000
Y_0	100000	111000	111000	111000
Y_1	000000	000000	000000	111000
X'	000111	000111	000111	000111
Y'_0	000100	000111	000111	000111
Y'_1	000000	000000	000000	000111

Table 4.4. Puncturing and repeating pattern for the tail bit periods. For rate 1/3, the puncturing table is read first from top to bottom repeating X and X', and then from left to right. For rate 1/5, the repeated coded symbols are X, X', Y_1, and Y'_1.

4.3.1.3.1.1 Turbo interleaver

The turbo interleaver, which is part of the turbo encoder, interleaves the N_{turbo} bits input to the turbo encoder. It is functionally equivalent to an approach (see Figure 4.3) in which the N_{turbo} input bits are written sequentially into an array at a sequence of addresses from 0 to N_{turbo}-1, and then the entire

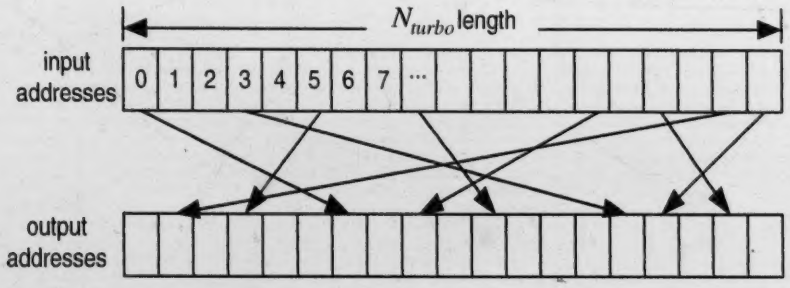

Figure 4.3. Interleaver structure.

sequence is read out from a sequence of addresses that are defined by the procedure described below:

1. Counter values (0 to 2^{n+5}-1) are written by rows into an array of 2^5 rows by 2^n columns, where $n = \lceil \log_2 N_{turbo} \rceil - 5$.

2. The elements within each row are permuted to $C(i)*(j+1)$, where indices i, j are the original row and column indices of the element, and $C(i)$ is a row-specific value from a table lookup (defined in Table 9.3.1.3.2.3.2.2-2 in [31]).

3. The rows are shuffled according to a bit-reversal rule. For example, for i=12 (01100), the bit reversed value of i is 5 (00110).

4. The elements in the array with values less than N_{turbo} are finally read out by columns. The new sequence consists of the interleaver output addresses.

4.3.1.3.2 Turbo decoder

Turbo decoder is based on an iterative application of maximum a posteriori (MAP) decoding to each constituent code.

A MAP decoder accepts as soft inputs the *a-priori log-likelihood ratio* (LLR) $L_a(X)$ and *soft channel input* { $L_c(X)$, $L_c(Y_0)$, $L_c(Y_1)$ } and delivers as soft output *a-posteriori LLR* of information bit which can be split into three terms: $L_a(X)$, $L_c(X)$ and *extrinsic information* $L_e(X)$. It makes possible the information exchange between decoders: each constituent decoder performs MAP decoding, and its outputs are used as the soft inputs for the next constituent decoder. Figure 4.4 demonstrates how soft information is forwarded/feed-backed inside the turbo decoder and how the turbo decoding works with the tail bits appending/removing.

Superscripts 1 and 2 are used in this figure to differentiate the *a-priori* and *extrinsic information* for MAP1 and MAP2, which correspond to the Constituent Encoder 1 and 2 in Figure 4.2, respectively.

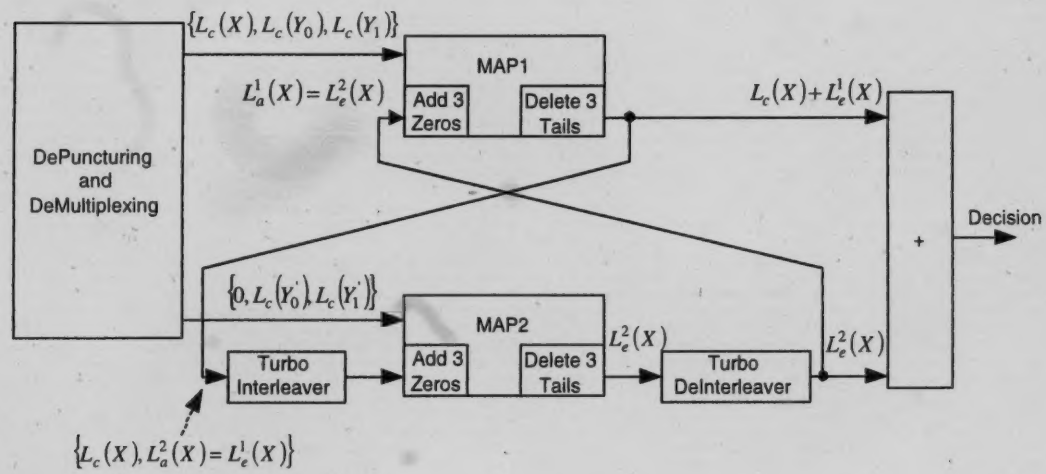

Figure 4.4. Turbo decoder.

The turbo decoder operates in serial mode (i.e., the MAP1 decoder processes before the MAP2 decoder starts operation). The turbo decoder operates as described below:

1. In the first step, the *a-priori probability* is unavailable. An equally likely assumption is made by setting $L_a^1(X) = 0$.

2. The MAP1 decoder takes in the *channel soft input* { $L_C(X)$, $L_C(Y_0)$, $L_C(Y_1)$ } from the upper branch of the DeMUX, and the zero *a-priori*. It updates the *a-posterior probability* of the information bit based on its code constraint and then delivers both the *channel soft input* and the extrinsic information, $L_C(X)+L_e^1(X)$, as soft input to MAP2.

3. The systematic bit X of the constituent Encoder 2 was punctured in the Puncturing and Multiplexing block at the transmit side. Hence, zero is inserted as $L_c(X)$ in the lower branch of DeMUX outputs, which is then sent as input to MAP2. Although DeMUX delivers zero $L_c(X)$ to the MAP2 decoder, MAP2 will learn its *channel soft input* of the systematic bit $L_c(X)$ from MAP1, along with the *a-priori LLR* $L_a^2(X)$ by taking $L_a^2(X)=L_e^1(X)$.

4. The *extrinsic* output $L_e^2(u)$ from MAP2 is interleaved and fed back to MAP1.

5. Subsequently, MAP1 has available an estimation of the *a-posteriori LLR*. It may consider this as *a-priori LLR* of its information bit X, i.e. $L_a^1(X)=L_e^2(X)$, and update it as the new log-likelihood ratio.

6. This process continues until a desired performance is achieved, at which point a final decision is made by comparing the final log-likelihood ratio $L_c(X)+L_e^1(X)+L_e^2(X)$ to zero.

It should be noted that each constituent MAP decoder works on both encoded data symbols and tail symbols. As the two don't share the 6-bit tail, the *a-priori LLR* values for the 6 tail bits will remain at zero during iterations. Thus, the output from each constituent MAP decoder shall be deleted the 3 tail bits, whereas at the input to each constituent MAP decoder, three zeros shall be appended (see Figure 4.4).

4.3.1.4 Signal constellations and spreading

The modulator generates in-phase and quadrature streams of QPSK, 8PSK, 16QAM or 64QAM modulation symbols, depending on the data rate. The signal constellations for the four modulation schemes are shown in Figures 4.5 – 4.8.

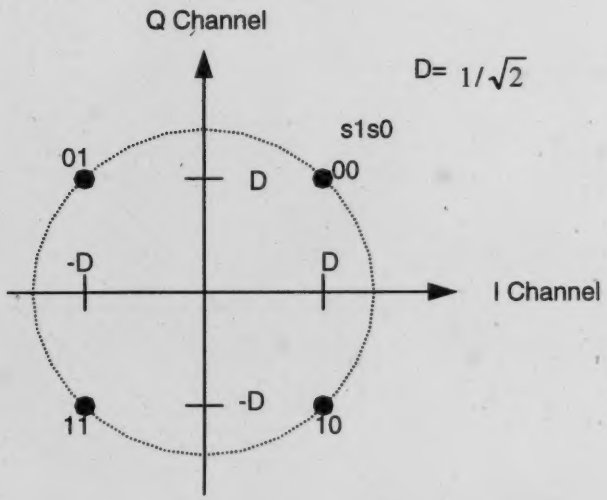

Figure 4.5. Signal constellation for QPSK modulation.

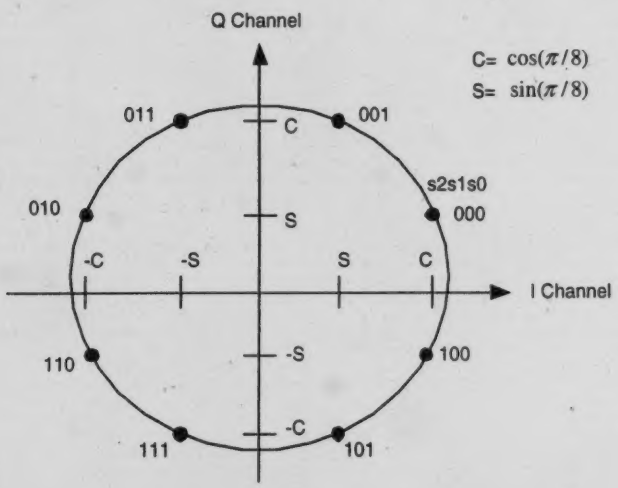

Figure 4.6. Signal constellation for 8PSK modulation.

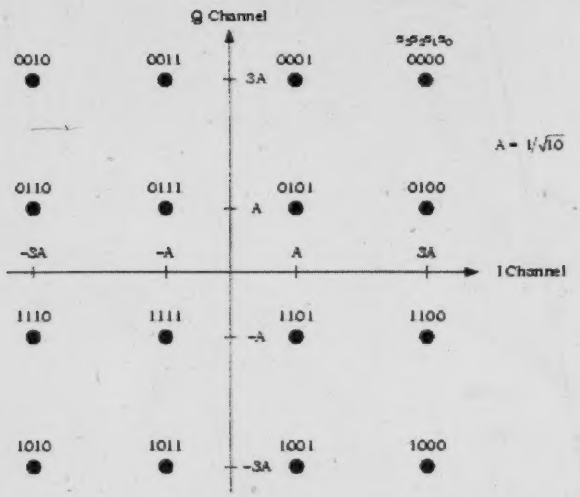

Figure 4.7. Signal constellation for 16QAM modulation.

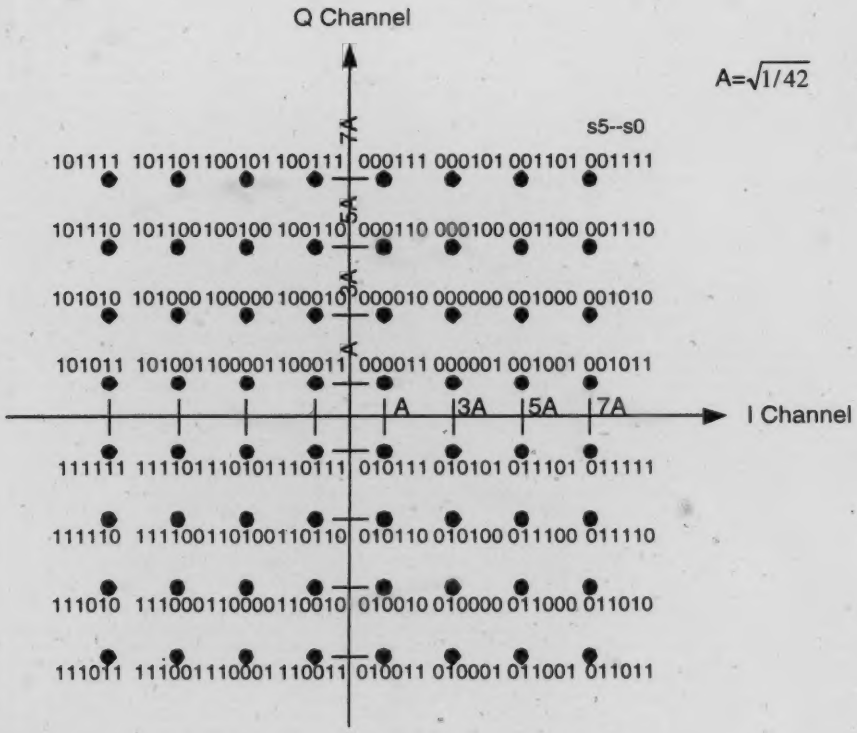

Figure 4.8. Signal constellation for 64QAM modulation.

4.3.1.4.1 HDR forward traffic channel spreading

In the HDR Forward Traffic Channel, the modulated symbols after channel interleaver are repeated or punctured as necessary. The resulting sequences of modulation symbols are de-multiplexed to form 16 pairs (in-phase and quadrature) of parallel streams. Each of the parallel streams is then spread with a distinct 16-ary Walsh function to yield Walsh symbols at rate 76.8ksp/s (or chip rate of 1228.8kcp/s). After that, the Walsh-coded symbols of all the streams are summed together at the chip level to form a single in-phase stream and a single quadrature stream at a chip rate of 1.2288 Mcp/s.

The resulting chips are time-division multiplexed (without changing the chip rate) with the preamble, Pilot Channel, and MAC Channel chips for the quadrature chip level scrambling operation. The scrambling sequence is a quadrature sequence of length 2^{15} (i.e., 32768 PN chips long). This sequence is called the *pilot PN sequence* and is generated by the following characteristic polynomials:

$P_I(x)=x^{15}+x^{10}+x^8+x^7+x^6+x^2+1$ (in-phase sequence I-PN)

$P_Q(x)=x^{15}+x^{12}+x^{11}+x^{10}+x^9+x^5+x^4+x^3+1$ (quadrature-phase sequence Q-PN)

4.3.1.4.2 1XTREME forward shared channel spreading

In the 1XTREME Forward Shared Channel, the modulated symbol sequences are serial-to-parallel converted to form up to 14 pairs (in-phase and quadrature) of parallel streams. Each of the parallel streams is later spread with one of fourteen 16-ary Walsh codes (W_2^{16} to W_{15}^{16}) to yield Walsh symbols at rate 76.8ksp/s (or chip rate of 1228.8 kcp/s); one Walsh symbol per modulation symbol is used. Following orthogonal spreading, the modulation sequence is quadrature scrambled by a quadrature pilot PN sequence of length 2^{15} (i.e., 32768 PN chips in length) generated by the following characteristic polynomials:

$P_I(x)=x^{15}+x^{13}+x^9+x^8+x^7+x^5+1$ (for the in-phase sequence IPN)

$P_Q(x)=x^{15}+x^{12}+x^{11}+x^{10}+x^6+x^5+x^4+x^3+1$ (for the quadrature-phase sequence QPN)

Each of up to 14 orthogonal Walsh code channels assigned to packet data traffic is assigned 1/14 of the power allocated to the traffic channels; 80% of the total sector transmit power is allocated to the traffic channels. Hence, effectively, the signal carrying the packet data traffic experiences processing gain of 16/14, or 0.58dB. In other words, spreading the modulation symbols by a factor of 16 in each of the 14 orthogonal code channels reduces the symbol energy required to achieve a given PER by a factor of 16/14 in comparison to a link without spreading using the same modulation/coding scheme and symbol rate. The spreading and scrambling operations are not explicitly implemented in the link level simulations. The processing gain is taken into account at the system level.

4.3.1.5 Slot and code channel structure

4.3.1.5.1 HDR forward channel structure and slot structure

The Forward Traffic Channel data modulation chips are time-division multiplexed with the Preamble, Pilot Channel, and MAC Channel chips as shown in Figure 4.9; the chip rate of 1228.8kcp/s is preserved in the TDM operation. All time-division-multiplexed channels are transmitted at the maximum power of the sector. Forward Traffic Channel Physical Layer packets are transmitted in 1 to 16 slots. The Forward Traffic Channel data symbols fill the slots as shown in Figure 4.10. Due to the 16-way parallelizing operation and subsequent 16-ary Walsh spreading and chip-wise addition of parallel streams, effectively each chip carries one QPSK, 8PSK or 16QAM symbol.

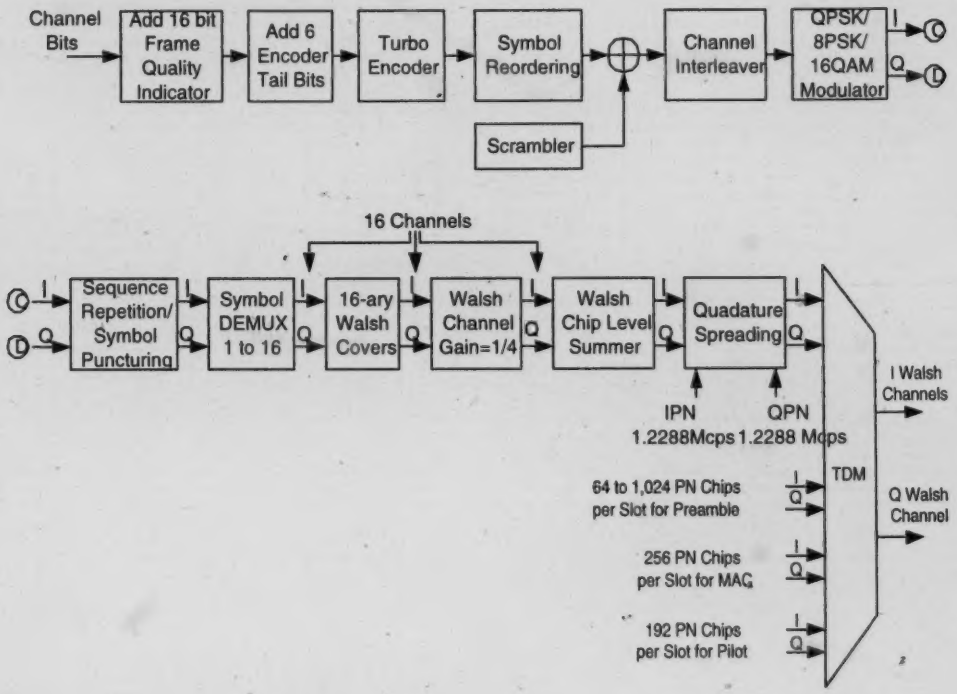

Figure 4.9. HDR forward channel structure.

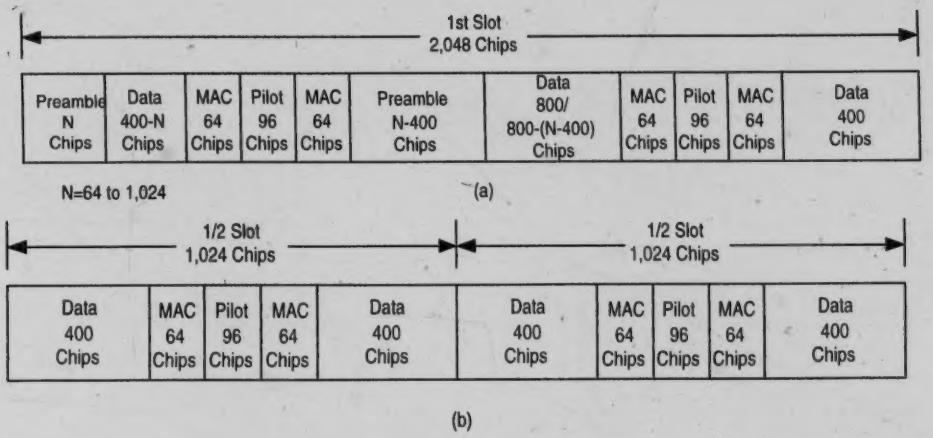

Figure 4.10. HDR forward channel active slot structure (a) the first slot (b) the non-first slot for multi-slot transmission.

A slot during which no traffic is transmitted is referred to as an idle slot. Idle slot structure is shown in Figure 4.11. During an idle slot, the sector transmits only the Pilot Channel and the MAC Channel.

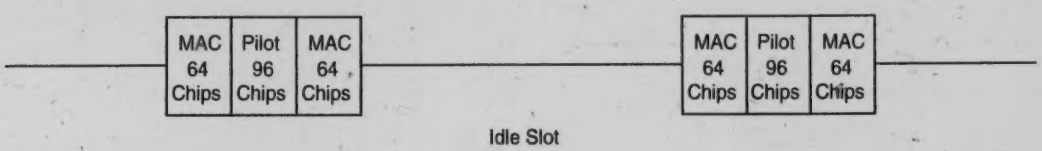

Figure 4.11. HDR forward channel idle slot structure.

4.3.1.5.2 1XTREME code channel structure

The 1XTREME Forward Shared Channel structure is shown in Figure 4.12.

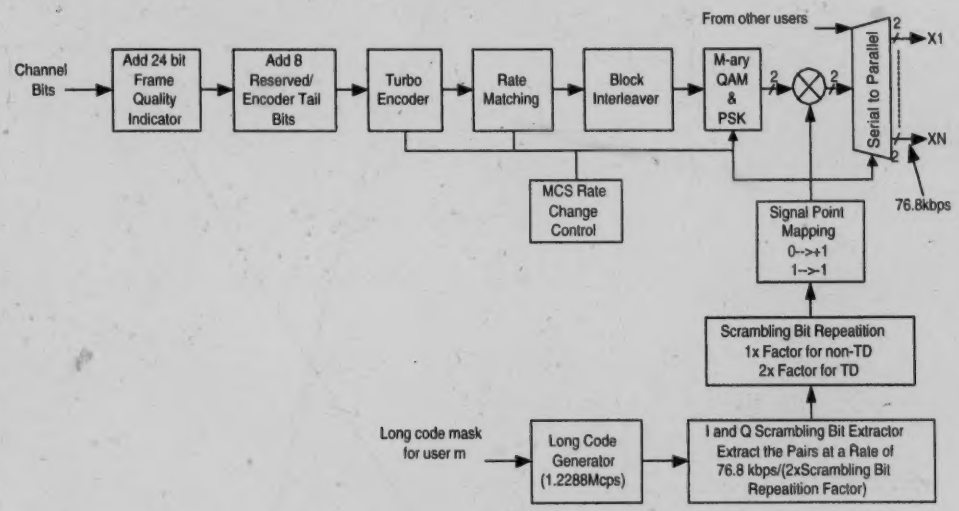
From other users
Channel Bits
Add 24 bit Frame Quality Indicator
Add 8 Reserved/ Encoder Tail Bits
Turbo Encoder
Rate Matching
Block Interleaver
M-ary QAM & PSK
Serial to Parallel
X1
XN
76.8kbps
MCS Rate Change Control
Signal Point Mapping 0-->+1 1-->-1
Scrambling Bit Repeatition 1x Factor for non-TD 2x Factor for TD
Long code mask for user m
Long Code Generator (1.2288Mcps)
I and Q Scrambling Bit Extractor Extract the Pairs at a Rate of 76.8 kbps/(2xScrambling Bit Repeatition Factor)

Figure 4.12. 1XTREME forward shared channel structure.

4.3.1.6 Hybrid ARQ for HDR

The HDR Forward Channel employs Type II Hybrid Automatic Repeat Request (ARQ) scheme. The hybrid ARQ scheme employs turbo codes as inner forward error correction (FEC) codes, and cyclic redundancy check (CRC) codes as outer error detection codes. It also takes advantage of incremental redundancy and soft packet combining. The application of type II hybrid ARQ allows for bit rate adaptation to the current radio channel conditions even after the specific transmission format (modulation & coding, and packet size) is selected. Due to the inclusion of incremental redundancy in the HDR hybrid ARQ scheme, it

needs to be simulated at the link level, leading to the need for considering link level performance of 41 transmission formats as listed in Table 4.1.

The HDR Forward Channel uses multi-slot transmission with 4-slot interlacing. The consecutive slots allocated for transmission of a given packet are separated by 3 slots allocated to other transmissions. If a positive is received on the reverse link ACK Channel and the Physical Layer packet has been received before all of the allocated slots have been transmitted, the remaining reserved slots are made available to the next Physical Layer packet transmission. Figure 4.13 illustrates the multi-slot interlacing approach for the 153.6kbps data rate case where 4 slots per packet are used. In this case, up to 4 re-transmissions are allowed.

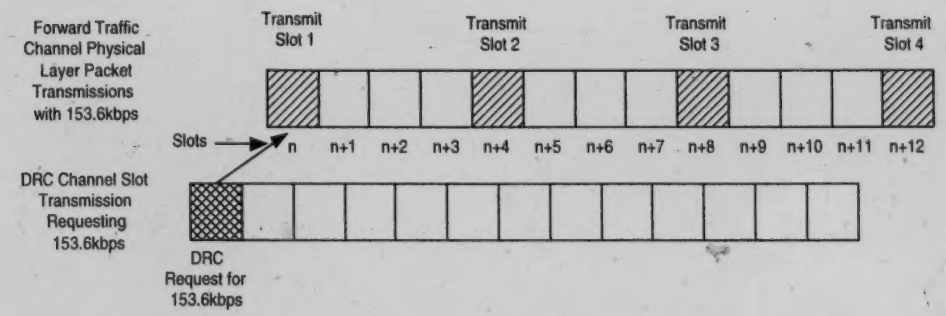

Figure 4.13. Example of slot interlacing for multi-slot packet transmission in HDR forward channel.

Hybrid ARQ scheme used in 1XTREME does not employ incremental redundancy, and therefore it is easy to account for its function at the system level. Hence, it is not simulated at the link level.

4.3.1.7 Soft packet combining and incremental redundancy

The HDR Forward Traffic Channel uses soft packet combining and incremental redundancy to achieve slot-by-slot data rate adaptation to the channel conditions. The Physical Layer packet is first encoded using a rate 1/3 or 1/5 turbo code. With the selected modulation and coding scheme (MCS), the initial slot transmission of the packet consists of only those encoded bits that fit in the slot (Figure 4.10-a). On receiving a negative acknowledgement (NACK) for the packet, incremental amounts of redundancy (i.e., the remaining parity bits of the encoded data) are transmitted. If all the encoded data have been transmitted, the cycle is repeated, starting again with the very first coded bit. On receiving a positive acknowledgement (ACK) for the packet before the maximum allowed number of re-transmissions (slots), the current Physical Layer packet transmission stops and the next Physical Layer packet transmission starts. This procedure effectively matches the code rate and bit rate to the channel SINR. In addition, the transmission of parity bits dispersed in time provides a diversity gain during decoding. Soft packet combining and incremental redundancy operations require the receiver to store soft information corresponding to the Physical Layer packets that have not yet been decoded successfully. Each time the receiver obtains a repetition of coded bits, it combines them with previously stored soft information corresponding to the same coded bits. This process is repeated until the receiver has acummulated sufficient SINR to allow correct decoding to be performed.

4.3.1.8 AWGN performance evaluation and its relevance

In our link level simulations PER vs. E_s / N_o curves in AWGN are determined for all HDR and 1XTREME transmission formats, as listed in Tables 4.1 and 4.2. Not all functions depicted in Figs. 4.9 to 4.12 are relevant to such performance evaluation. Figures. 4.14 and 4.15 show the functional modules of the HDR and 1XTREME forward channel transmitter relevant to the AWGN performance evaluation.

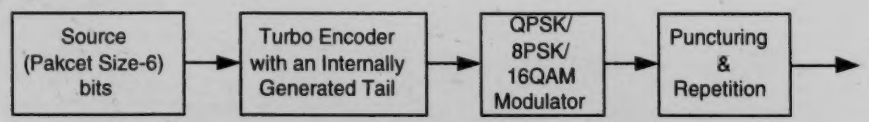
Source (Pakcet Size-6) bits
Turbo Encoder with an Internally Generated Tail
QPSK/ 8PSK/ 16QAM Modulator
Puncturing & Repetition

Figure 4.14. HDR forward traffic channel structure in simulation.

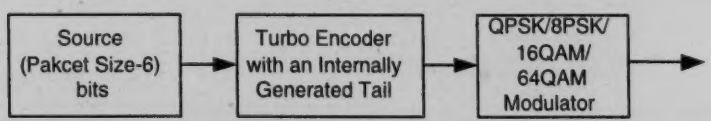

Figure 4.15. 1XTREME forward shared channel structure in simulation.

The PER curves obtained from AWGN link level simulations will be used at the system level for transmission format selection and packet erasure determination. In spite of the fact that the HDR and 1XTREME systems operate over fading mobile radio channels, AWGN link level curves can be used to simplify system level simulations due to the fact that both HDR and 1XTREME use very short transmission bursts over which the SIR seen by the mobile receiver is either constant, or can be represented as constant for the purpose of transmission format selection or packet erasure determination.

4.3.2 PER vs. E_s/N_0 curves in AWGN

A packet error rate (PER) curve vs. E_s / N_o in an AWGN channel is created using the link level simulation for each data rate, modulation and coding scheme given in Tables 4.1 and 4.2.

4.3.2.1 HDR forward traffic channel PER curves

Figures A.1 to A.6 in Appendix A present PER AWGN curves obtained after 8 iterations of the turbo decoder for all transmission formats and bit rates specified in Table 4.1. In the figures, data rate in kb/s, physical layer packet size in bits, and maximum allowable number of transmission slots are denoted as R, M_p, and S, respectively. Figures A.7 to A.11 compare the HDR Forward Traffic Channel PER curves corresponding to the same bit rate transmissions in different formats.

4.3.2.2 1XTREME forward shared channel PER curves

The PER vs. E_s / N_o curves for the cases of N = 2,…,10 can be obtained from those in Figure A.7. Due to the absence of incremental redundancy in 1XTREME, these curves will be the same as those in Figure A.7, except the corresponding values of E_s / N_o will be reduced by a factor N (on a linear scale). The processing gain of 16/14 is notincluded in the link-level curves, and will be accounted for in system level simulations.

4.4 Summary

The general structure of the HDR and 1XTREME simulations was depicted in Figure 4.1. The link-level and system level simulations are performed separately. The link-level simulation involves the modeling of the most relevant functional block diagrams of the channel structure for HDR and 1XTREME, including Turbo encoder/decoder, modulator/demodulator, and repetition/puncturing operations. The AWGN channel is assumed for the link-level simulations due to the short-time duration of the packets. The fading channel is practically time-invariant in these short periods of time, and hence it behaves as an AWGN channel. In the following chapter the description of the system level simulator will be presented.

Table C-2: PASS Age Comparisons - Subscale Raw Scores
Two-Factor ANOVA Data

PASS General Ability

SOURCE	*DF*	*SS*	*MS*
Age	1	0.2	0.2
Retention/Promotion	1	15.6	15.6
*Interaction(Age*R/P)*	1	30.6	30.6
Error	36	445.9	12.4
Total	39	492.4	

F(Age) = 0.02
F(RetProm) = 1.26
F(A*B) = 2.47

PASS Arithmetic

SOURCE	*DF*	*SS*	*MS*
Age	1	11.02	11.02
Retention/Promotion	1	0.22	0.22
*Interaction(Age*R/P)*	1	2.03	2.03
Error	36	329.5	9.15
Total	39	342.77	

F(Age) = 1.20
F(RetProm) = 0.02
F(A*B) = 0.22

PASS Reading / Spelling

SOURCE	*DF*	*SS*	*MS*
Age	1	14.4	14.4
Retention/Promotion	1	3.6	3.6
*Interaction(Age*R/P)*	1	0.1	0.1
Error	36	641	17.8
Total	39	659.1	

F(Age) = 0.81
F(RetProm) = 0.20
F(A*B) = 0.01

PASS Penmanship

SOURCE	*DF*	*SS*	*MS*
Age	1	0.4	0.4
Retention/Promotion	1	16.9	16.9
*Interaction(Age*R/P)*	1	1.5	1.6
Error	56	383	10.6
Total	59	401.9	

F(Age) = 0.04
F(RetProm) = 1.59
F(A*B) = 0.15

PASS School Satisfaction

SOURCE	*DF*	*SS*	*MS*
Age	1	13.23	13.23
Retention/Promotion	1	0.03	0.03
*Interaction(Age*R/P)*	1	15.63	15.63
Error	36	237.1	6.59
Total	39	265.98	

F(Age) = 2.01
F(RetProm) = 0.00
F(A*B) = 2.37

PASS Confidence

SOURCE	*DF*	*SS*	*MS*
Age	1	14.4	14.4
Retention/Promotion	1	1.6	1.6
*Interaction(Age*R/P)*	1	8.1	8.1
Error	36	251.8	6.99
Total	39	275.9	

F(Age) = 2.06
F(RetProm) = 0.23
F(A*B) = 1.16

Appendix D: Research Question #3, Gender Differences

Table D-1: PASS Gender Comparisons—Full Scale Raw Scores
Two-Factor ANOVA Data

SOURCE	*DF*	*SS*	*MS*
Gender	1	12	12
Retention/Promotion	1	43	43
*Interaction(Gend*R/T)*	1	66	66
Error	56	7961	142
Total	59	8083	

F(Gender) = 0.08
F(RetProm) = 0.30
F(A*B) = 0.46

Table D-2: PASS Gender Comparisons - Subscale Raw Scores
Two-Factor ANOVA Data

PASS General Ability

SOURCE	*DF*	*SS*	*MS*
Gender	1	0.3	0.3
Retention/Promotion	1	9.6	9.6
*Interaction(Gend*R/T)*	1	0.6	0.6
Error	56	605.5	10.8
Total	59	615.9	

F(Gender) = 0.03
F(RetProm) = 0.89
F(A*B) = 0.06

PASS Arithmetic

SOURCE	*DF*	*SS*	*MS*
Gender	1	8.82	8.82
Retention/Promotion	1	10.42	10.42
*Interaction(Gend*R/T)*	1	2.82	2.82
Error	56	540.53	9.65
Total	59	562.53	

F(Gender) = 0.91
F(RetProm) = 1.08
F(A*B) = 0.29

PASS Reading / Spelling

SOURCE	*DF*	*SS*	*MS*
Gender	1	0.2	0.2
Retention/Promotion	1	2.8	2.8
*Interaction(Gend*R/T)*	1	18.1	18.1
Error	56	695.5	12.4
Total	59	716.6	

F(Gender) = 0.02
F(RetProm) = 0.23
F(A*B) = 1.46

PASS Penmanship

SOURCE	*DF*	*SS*	*MS*
Gender	1	35.3	35.3
Retention/Promotion	1	0.3	0.3
*Interaction(Gend*R/T)*	1	4.3	4.3
Error	56	628.9	11.2
Total	59	668.7	

F(Gender) = 3.15
F(RetProm) = 0.03
F(A*B) = 0.38

PASS School Satisfaction

SOURCE	*DF*	*SS*	*MS*
Gender	1	14	14
Retention/Promotion	1	0.8	0.8
*Interaction(Gend*R/T)*	1	10.4	10.4
Error	56	571.7	10.2
Total	59	597	

F(Gender) = 1.37
F(RetProm) = 0.08
F(A*B) = 1.02

PASS Confidence

SOURCE	*DF*	*SS*	*MS*
Gender	1	0.6	0.6
Retention/Promotion	1	2.4	2.4
*Interaction(Gend*R/T)*	1	6.67	6.67
Error	56	169.07	3.02
Total	59	178.73	

F(Gender) = 0.20
F(RetProm) = 0.79
F(A*B) = 1.02

Appendix E: Some Relationships Between Personality Type And Academic Self-Perception

Of the 245 children administered the PASS in the thesis group, 231[1] were also given the *Murphy-Meisgeier Type Indicator for Children* (MMTIC) (Meisgeier & Murphy, 1987). These children formed the study group which was used to examine three questions related to the MMTIC. First, this appendix study examined Meisgeier and Murphy's concepts of Clear versus Undifferentiated type preferences, paying particular attention to, and testing the authors' hypothesis that the consolidation of clear type preference is a function of development. Second, the relationship between Clear versus Undifferentiated type preferences, and grade promotion/non-promotion was examined using a series of two-way ANOVAs for comparison purposes. The research question for the second segment, then was this: What is the academic self-concept of the child as it relates to the establishment of type and the effects of grade retention or continuous promotion. Lastly, as a sidebar to the retention/ promotion issues studied in the thesis, a comparison was made of the self-perception of academic ability among children of different personality types. This final inquiry was based upon the following question: Are there differences in the self-perception of academic ability among children of different personality types in the clinical samples?

The MMTIC (Meisgeier & Murphy, 1987) is a self-report instrument used to help establish the type preference of children, based upon the model of the *Myers-Briggs Type Indicator* (MBTI) (Myers & McCaulley, 1985). The MMTIC is made up of 70 items, each of which is formatted so that the subject must choose one of two answers.

---

[1] Only one of the children given the MMTIC was six years old. For grouping purposes and because the MMTIC was standardized using children in Grades Two to Eight, this subject was dropped from the study, leaving a total of $N = 230$.

For example, an item from the Introvert-Extrovert Preference Scale is, "You like to have: a) Lots of friends, b) A few close friends." The authors of the MMTIC have attempted to show the relevance of the MMTIC in educational situations. The Applications chapter of the manual provides teachers with methods for applying type theory in the classroom by giving teachers strategies to use with children of the various types.

Isabel Briggs Myers, the major author of the MBTI, fashioned the instrument by expanding the type theory of C. G. Jung. Jung (1971) suggested that differences in behavior were the result of preferences related to the way our personalities function to meet the demands of daily living. Myers expanded Jung's original typology to include four pairs of preference alternatives:

Extroverted versus Introverted

Sensing versus Intuitive

Thinking versus Feeling

Judging versus Perceiving

The 16 type categories that arise from these dichotomies form the basis of Myers' type theory. While it is stressed that the alternatives are not "written in stone" but are preferences, subjects are placed in categories according to type.

Unlike the MBTI, however, type preference in the MMTIC is not totally categorical. If a child's score is less than one standard deviation on either side of the scale's midpoint, it is considered to be within the U-band range and the child's type preference is said to be *undetermined*. Because the study of psychological type was not a major focus of the thesis, a detailed discussion of type theory or a description of the 16 psychological types will not be included. The reader is pointed to *Gifts Differing, 10th Anniversary Edition* by Isabel Briggs Myers (1990) and the MBTI Manual (Myers &

McCaulley, 1985). However, to provide a backdrop for the assumption by Murphy and Meisgeier that type preference is a function of the child's development, a very brief examination of the developmental views of Jung and Myers follows.

While not discounting environmental influences, Jung (1971) observed that children often are disposed to exhibiting a typical attitude very early in life. He noted that two young children in the same family may manifest contradictory or different attitudes. Ultimately, Jung asserted, "it must be the individual disposition which decides whether the child will belong to this or that type despite the constancy of external conditions" (Jung, 1971, p. 332). When the individual disposition of the child is violated, by the influence of a domineering parent, for example, the person is likely to become neurotic at a later point. Jung concluded that attempts to reverse the dispositional order usually are harmful to the individual.

Following Jung's theory, Isabel Briggs Myers (1990) hypothesized that type preference is innate and is in-born like left- and right-handedness. Myers suggested that preference can manifest itself at a very young age. For example, the "young thinker [as opposed to feeling type], even at two years old, will do things for reasons but sees no point in doing them for love" (Myers, 1990, p. 169). But at the same time, Myers states that the four processes are used almost at random by young children—until they learn how to differentiate. It is this latter view that Meisgeier and Murphy (1987) develop in the MMTIC. This assumption is tested in the first study of this appendix.

METHOD

In this section of the appendix, the procedures used in each of the three studies will be discussed. The statistical formats of the studies in this paper were similar to those of the main body of the thesis. For example, the comparison groups in Study Question #2 were composed of repeaters and non-repeaters. ANOVAs and *t* statistics were used in the statistical analyses.

MMTIC Study Question #1: Clear and Undetermined Type

One of the assumptions upon which the MMTIC is based, is that the child's dominant function is still developing throughout the early years of the child's schooling. The authors of the MMTIC attempted to account for this lack of dominant function differentiation by using the Undetermined category which is stated in terms of the U-Band; the child whose choice of preference has not been clearly determined is said to score in the U-band. Of the 1506 respondents in the MMTIC standardization group, 578 (38.38%) children showed clear type with no scores falling in the U-band on each of the four scales (EI, SN, TF, JP). The proportion of subjects in the clinical study exhibiting clear type, was compared with that of the MMTIC norm group.

The hypothesis that the child's type preference develops over time as part of overall growth, was tested using the children in the present clinical group. The children in the study were first grouped by age. Then a series of *chi*-square calculations were performed to compare the clear type versus undetermined type proportions of the various age groups with the proportion of the total study group (Clear = 108 versus Undetermined = 122).

A second test of the hypothesis that clear type preference is a function of development was set up. A sample of 20 children was randomly selected from subjects in the youngest quartile. Then a matched sample was selected from children in the oldest quartile. The mean age of the total number of subjects in the younger quartile was 7.92 and the mean age of the group in fourth quartile was 12.52. The subjects in the two age groups were matched according to the following criteria: a) referral to the Clinic for learning difficulties and b) equal gender proportions. The decision was made to use a sample of 20 from each of the first and fourth quartiles rather than all the subjects in each of the quartiles, because of the advantages afforded by matching. The gifted students and those referred only for behavioral or emotional difficulties were eliminated, creating more homogeneous groups for comparison purposes. The null hypothesis, then, stated that there would be no significant difference between the proportions of clear types and undetermined types among the two groups.

The selection process captured fifteen males and five females in each sample. In the younger sample, eight children showed clear type while the types of twelve of the subjects fell within the U-band. The older group revealed seven students with clear type and thirteen whose type was still not totally determined. A *chi*-square goodness of fit test was run, using the younger group's C/U ratio as the expected frequency [2] and the older group's numbers as the observed frequency.

MMTIC Study Question #2: Retained Versus Promoted Children

This phase of the MMTIC study returned to the major question of the thesis: Are there differences in the academic self-perception of those children referred to the Clinic who have repeated a school grade and those who have not repeated? The differences in

[2] Murphy and Meisgeier suggest that type becomes determined over the course of development. Therefore the younger group was chosen to offer the expected frequency. It should have fewer clear types than undetermined types. The exercise had a given conclusion, considering the fact that the older group had even fewer clear types (7 out of 20 versus 8 out of 20 for the younger group)

academic self-concept were examined in relation to whether or not clear type had been established in the child. The PASS results of a sample of children with clear type were compared with those of a sample in which at least two of the four scales fell into the U-band.

A series of two-way ANOVAs using four study groups provided the statistical basis for a comparison of differences in academic self-concept between retained and non-retained children of clear type preference and those of undetermined preference. The initial sample was a group of 15 students who had been asked to repeat a grade at least once in their school careers. Each of the children had failed to establish a clear type preference on at least two of the four MMTIC scales. Next a matched group of continuously promoted children with at least two scores in the U-band of the MMTIC was chosen. The final two samples were composed of children of clear type on the MMTIC. One sample of 15 had previously been retained and the other group of clear type had been promoted after each grade completed. Matching was based upon proportional numbers of males and females, and LD referrals. As in the main body of the thesis, the PASS means of the sample groups were next compared to the Full Scale and Subscale means of the PASS norm group using the *t* statistic.

MMTIC Study Question #3: INFPs Versus STs

As will be discussed in the Results section of Study Question #1, a significantly high proportion of the 230 children given the MMTIC exhibited a clear type preference when compared to the standardization group (Clear = 108 versus Undetermined = 122), $X^2 (1, N = 230) = 6.88, p < .01$. This group of 108 children formed the basis of the final component of the MMTIC study. The children were categorized as to type, and the results were placed into a type table. *Chi*-square calculations were employed with the results presented in Table E-10 at the end of this appendix. The study group showed

significantly different proportions from the MMTIC standardization group in three of the 16 type categories. The INFP typology had the greatest proportional over-representation in the clinical group when compared to the MMTIC norm group (21.30% versus 8.5%, $p < .001$). Also generating a larger proportion on the study group type table when it was compared to the MMTIC population, was the ISFP category (8.33% versus 3.5%, $p < .05$). The ESFJ group in the thesis study had a significantly smaller proportion than its MMTIC norm group counterpart (7.41% versus 16.3%, $p < .05$).

When only the students referred for learning difficulties ($n = 86$) were compared to the MMTIC standardization group, the same three types (INFP, ISFJ, ESFJ) reached proportions which led to levels of significance (see Table E-11 at the end of the paper for results of the LD analysis). The proportion of INFP children increased in this analysis dealing only with children referred for learning difficulties (up to 24.42% from 21.30% when $n = 108$). Since about 80% of the children in the clear group were referred as LD, it appears that there may be a relationship between the INFP typology and difficulties in school-related tasks.

To examine the relationship between the INFP typology and perceived problems in school-related tasks, an attempt was made to set up a study using the PASS Raw Scores of a sample of clear INFP children with subjects of the typology expressing the greatest polar differences possible. The natural choice for the subjects of this contrasting group would be ESTJ children. The type table for the thesis MMTIC group, however, yielded only seven ESTJ subjects. The decision was therefore made to increase the sample size by using as a study group the twelve children registered as ST and who had stated clear type preference. The academic self-perception of these ST were compared with a group of INFP subjects, matched for age, gender, and proportion of students who had been held back in a grade during their schooling. Of the 12 children in the ST

sample, only one had repeated a grade. Because of this low number, it was not feasible to compare repeaters and non-repeaters in this segment of the thesis. Table E-1 provides a description of the two groups in this part of the study. First, a series of one-way ANOVAs compared the PASS Full Scale and Subscale scores of the two groups. Then, continuing the statistical format of the thesis, the PASS means of the two samples were compared to the means of the PASS standardization groups using the appropriate *t* statistic.

Table E-1: INFPs Versus STs : Descriptive Data

SAMPLE GROUPS	*n*	*MEAN AGE*	*TYPE BREAKDOWN*	*GENDER*
INFPs	12	9.81	**INFP's - 12**	M=7, F=5
STs	12	9.85	**ESTJs - 7** **ISTPs - 3** **ISTJs - 1** **ESTPs - 1**	M=7, F=5

RESULTS

The results of the three studies are presented below. These are followed by a brief discussion of the findings of the comparisons.

MMTIC Study Question #1: Clear and Undetermined Type

When compared to the MMTIC standardization group, the present clinical group had a significantly larger proportion of subjects who manifested clear type (46.96%) on the four scales of the MMTIC (Clear = 108 versus Undetermined = 122), X^2 (1, N = 230) = 6.88, $p < .01$. Of the 108 children demonstrating clear type, 86 (80%) had been referred to the Clinic for learning problems.

One of the suppositions held by the authors of the MMTIC is that the child's type preference develops over time as part of overall growth. Therefore it should follow that as the child matures, there will be less likelihood that his or her test scores will fall within the U-band. This hypothesis was tested using the children in the present clinical group. The results are presented in Table E-2. In the present study, the only age group in which subjects showed a significantly high clear type preference was the ten year-old group (Clear = 29 versus Undetermined = 18), X^2 (1, n = 47) = 4.10, $p < .05$. As Table E-2 shows, all the groups, both younger and older than the ten year-old group had smaller proportions of clear type preference in relation to undetermined preference.

In the second test of the hypothesis that type preference develops over time, a sample of 20 children was randomly selected from subjects in the youngest quartile. Then a matched sample was selected from children in the oldest quartile. The resulting comparisons revealed no significant differences between the proportions of clear and undetermined types in each group.

Table E-2: MMTIC Age Samples:
Clear Versus Undetermined Type Preference

AGE GROUPS [a]	*n*	*CLEAR TYPE*	*UNDETER-MINED*	*% CLEAR TYPE*	*% UNDE-TERMINED*	X^2 [b]
7 Yr-Olds	23	13	10	56.52	43.48	0.84
8 Yr-Olds	47	23	24	48.94	51.06	0.07
9 Yr-Olds	47	18	29	38.30	61.70	1.41
10 Yr-Olds	47	29*	18	61.70*	38.30	4.10*
11 Yr-Olds	30	15	15	50.00	50.00	0.11
12 Yr-Olds	22	6	16	27.27	72.73	3.42
13 Yr-Olds	5	1	4	20.00	80.00	1.46
14 Yr-Olds	9	3	6	33.33	66.67	0.67
TOTALS	230	108	122	46.96	53.04	

NOTE: a) Because there was only one six year-old, she was dropped
b) X^2 calculation for each age group is based upon overall totals of clinical group (N =230, Clear Type =108, Undetermined = 122)
* Proportion of 10 year-olds showing Clear Type significantly higher than overall totals at the $p < .05$ level.

In summary, the study of the MMTIC Clear/Undetermined type ratios found no evidence to suggest that type becomes differentiated into four clear preferences over time. A movement toward clear type culminated at age ten, but a drop-off occurred as the older groups were examined. The lower proportions of Clear type preferences among the 13 and 14 year-olds may be a result because of the smaller numbers of children in the older age groups in the PASS population. Since the PASS was normed for children in Grades Three to Six, many of the older children referred to the Clinic were not given the MMTIC. Further research investigating the proportions of Clear and Undetermined type preferences in the older age groups would appear to be warranted, as the results of the present study may be related to the fact that most of the children were referred because of learning difficulties.

MMTIC Study Question #2: Retained Versus Promoted Children

The outcomes of the two-way ANOVAs failed to demonstrate any significant differences among the four groups on any of the PASS scales when the grade retained children were compared with those who had been continuously promoted. The variance seen on the PASS scores led to rather high error factors (and non-significant results) when the ANOVAs were calculated. Tables E-8 and E-9 at the end of this appendix show the results of the ANOVAs.

When the four groups were compared to their counterparts in the PASS normative study, the retained children of undetermined type generally rated themselves lower than the other three groups. On the Perception of Reading/Spelling scale, the mean Raw Score of the sample containing repeaters of undetermined type showed the greatest significant difference, $t\ (14) = -3.19, p < .01$. The group consisting of continuously promoted students of clear type did not differ significantly from the PASS standardization group on any of the PASS scales. Table E-3 shows descriptive statistics for the Raw Score Means and Standard Deviations for the four groups selected for the above comparisons.

MMTIC Study Question #3: INFPs Versus STs

Significant differences were demonstrated when the ANOVAs comparing the ST and INFP children were analyzed. The ST children rated themselves stronger than did the INFP subjects on each of the PASS Scales, and significantly so on five of the seven Scales. It should be noted that the INFP/ST comparison was the only ANOVA series of the thesis in which significant differences were noted. It was also the only set of ANOVAs in which grade promotion versus grade retention did not form the basis for the

Table E-3: MMTIC Clear versus Undetermined Type Comparisons
PASS Raw Scores :Means and Standard Deviations

SAMPLE GROUP	FULL SCALE	GENERAL ABILITY	ARITH-METIC	READING SPELLING	PENMAN -SHIP	SCHOOL SATISFACTION	CONFID -ENCE
Retained With At Least Two Score In U-Band	**38.47***	**7.20**	**9.33**	**6.20****	**5.67***	**7.13**	**3.47***
	12.70	4.00	2.58	3.43	3.66	3.02	1.96
Non-Repeating With At Least Two Scores In U-Band	**41.40**	**6.87**	**8.87**	**6.80***	**8.27**	**6.80**	**3.53***
	11.96	2.61	3.14	3.45	2.52	3.61	1.77
Retained With Clear Type	**38.33***	**6.20**	**8.40**	**6.20***	**6.60**	**6.87**	**3.80**
	14.43	3.57	3.81	4.28	3.02	3.14	1.74
Non-Repeating With Clear Type	**39.73**	**7.80**	**7.80**	**7.27**	**6.93**	**5.93**	**3.60**
	12.31	3.47	4.09	4.03	2.52	2.69	1.88

NOTE: a) Boldface type values denote *means*. Lightface type values denote *standard deviations*.
b) Statistical analysis assumed two-tailed tests.
c) Significance levels based upon differences between sample means and PASS normative data.
* $p < .05$ ** $p < .01$ *** $p < .001$

comparison. The results reaching significance are summarized in Table E-4.

Next the sample groups were matched with the PASS standardization group using *t* statistic calculations. The results of the *t* calculations reinforced the ANOVA findings. While averages of the scores of the 12 ST subjects did not differ from the PASS norm group on any of the seven PASS Scales, the means of the INFP children were significantly below those of the PASS norm group on each of the seven scales. The INFP students rated themselves particularly low on the PASS Full Scale, $t = -5.20, p < .001$, and the Confidence Scale, $t = -5.36, p < .001$. It is interesting that this analysis of the ST and INFP type groups produced differences which were much more clear

Table E-4
INFP Versus ST: Significant ANOVA Results

STs SIGNIFICANTLY HIGHER ON THESE PASS SCALES
Full Scale - $F(1,22) = 12.24, p < .01$
Arithmetic - $F(1,22) = 5.89, p < .05$
Reading/ Spelling - $F(1,22) = 4.21\ p < .05$
School Satisfaction - $F(1,22) = 5.36\ p < .05$
Confidence - $F(1,22) = 7.45\ p < .05$
STs HIGHER BUT NOT SIGNIFICANTLY SO (PASS SCALES)
General Ability - $p > .05$
Penmanship - $p > .05$

than any of the comparisons of grade-retained and promoted children. The sample means, standard deviations, and significant differences when compared to the PASS standardization group, are summarized in Table E-5.

CONCLUSION

All of the ANOVA comparisons of academic self-concept of children in the main body of the thesis were based upon the promotion/non-promotion model. Interestingly, the only substudy to produce significant ANOVA results, did not examine differences between children who had been continuously passed with those who had been asked to repeat a grade. It was the ANOVA comparison of the academic self-concept of a group of INFP subjects with ST children that proved to be the exception to a series of

Table E-5: Differences Between INFPs and STs
PASS Raw Scores—Means and Standard Deviations

SAMPLE GROUP	*FULL SCALE*	*GENERAL ABILITY*	*ARITH-METIC*	*READING SPELLING*	*PENMAN -SHIP*	*SCHOOL SATISFACTION*	*CONFID -ENCE*
INFPs	**30.42*****	**5.08****	**5.67*****	**5.25*****	**5.17*****	**5.25**	**2.25*****
	10.71	2.75	4.72	3.91	3.07	2.56	1.54
STs	**43.75**	**7.00**	**9.58**	**8.25**	**6.58**	**7.17**	**4.42**
	7.72	3.22	3.00	3.22	2.75	3.64	2.27

NOTE: a) Boldface type values denote *means*. Lightface type values denote *standard deviations*.
b) Statistical analysis assumed two-tailed tests.
c) Significance levels based upon differences between sample means and PASS normative data.
$^{**}p < .01$ $^{***}p < .001$

non-significant ANOVA results. Further research with large enough samples to study the academic self-concept of INFPs and ESTJs with learning difficulties matched according to level of academic achievement, could prove interesting.

References

Jung, C. G. (1971). *Psychological types* (H.G. Baines, Trans., Revised by R.F.G. Hull,). Princeton, NJ: Princeton University Press.

Meisgeier, C., & Murphy, E. (1987). *Murphy-Meisgeier Type Indicator for Children Manual*. Palo Alto, CA: Consulting Psychologists Press.

Myers, I. B., & McCaulley, M. H. (1985). *Manual: A guide to the development and use of the Myers-Briggs Type Indicator*. Palo Alto, CA: Consulting Psychologists Press.

Myers, I. B., with Myers, P. B. (1990). *Gifts differing: 10th anniversary edition*. Palo Alto, CA: Consulting Psychologists Press.

Table E-6: INFP Versus ST Students—PASS Comparisons—
One-Way ANOVA Data Based on Full Scale Raw Scores

SOURCE	*DF*	*SS*	*MS*
Factor	1	1066.7	122
Error	22	1917.2	87.1
Total	23	2983.8	

$F(1,22) = 12.24$
$p = 0.002$

Table E-7: INFP Versus SP Students - PASS Comparisons
One-Way ANOVA Data: Subscale Raw Scores

PASS General Ability

SOURCE	*DF*	*SS*	*MS*
Factor	1	22.04	22.04
Error	22	196.92	8.95
Total	23	218.96	

$F(1,22) = 2.46$
$p = 0.131$

PASS Arithmetic

SOURCE	*DF*	*SS*	*MS*
Factor	1	92.0	92.0
Error	22	343.6	14.6
Total	23	435.6	

$F(1,22) = 5.89$
$p = 0.024$

PASS Reading / Spelling

SOURCE	*DF*	*SS*	*MS*
Factor	1	54.0	54.0
Error	22	282.5	12.8
Total	23	336.5	

$F(1,22) = 4.21$
$p = 0.024$

PASS Penmanship

SOURCE	*DF*	*SS*	*MS*
Factor	1	12.04	12.04
Error	22	186.58	186.58
Total	23	198.63	

$F(1,22) = 1.42$
$p = 0.246$

PASS School Satisfaction

SOURCE	*DF*	*SS*	*MS*
Factor	1	45.38	45.38
Error	22	186.25	8.47
Total	23	231.63	

$F(1,22) = 5.36$
$p = 0.030$

PASS Confidence

SOURCE	*DF*	*SS*	*MS*
Factor	1	28.17	28.17
Error	22	83.17	3.78
Total	23	111.33	

$F(1,22) = 7.45$
$p = 0.012$

Table E-8: MMTIC Clear versus Undetermined Type Comparisons
PASS Full Scale Raw Scores: Two-Factor ANOVA Data

SOURCE	*DF*	*SS*	*MS*
U/C	1	12	12
Retention/Promotion	1	70	70
*Interaction(U/C*R/T)*	1	9	9
Error	56	9296	166
Total	59	9387	

F(U/C) = 0.07
F(RetProm) = 0.42
F(A*B) = 0.05

Table E-5: MMTIC Clear versus Undetermined Type Comparisons - PASS Subscale Raw Scores - Two-Factor ANOVA Data

PASS General Ability

SOURCE	*DF*	*SS*	*MS*
U/C	1	0	0
Retention/Promotion	1	6	6
*Interaction(U/C*R/T)*	1	14	14
Error	56	666.9	11.9
Total	59	687	

***F*(U/C) = 0.00**
***F*(RetProm) = 0.50**
***F*(A*B) = 1.18**

PASS Arithmetic

SOURCE	*DF*	*SS*	*MS*
U/C	1	15	15
Retention/Promotion	1	4.3	4.3
*Interaction(U/C*R/T)*	1	0.1	0.1
Error	56	669.1	11.9
Total	59	688.4	

***F*(U/C) = 1.26**
***F*(RetProm) = 0.36**
***F*(A*B) = 0.01**

PASS Reading / Spelling

SOURCE	*DF*	*SS*	*MS*
U/C	1	0.8	0.8
Retention/Promotion	1	10.4	10.4
*Interaction(U/C*R/T)*	1	0.8	0.8
Error	56	814.1	14.5
Total	59	826.2	

***F*(U/C) = 0.06**
***F*(RetProm) = 0.72**
***F*(A*B) = 0.06**

PASS Penmanship

SOURCE	*DF*	*SS*	*MS*
U/C	1	0.6	0.6
Retention/Promotion	1	32.27	32.27
*Interaction(U/C*R/T)*	1	19.27	19.27
Error	56	492.8	8.8
Total	59	544.93	

***F*(U/C) = 0.07**
***F*(RetProm) = 3.67**
***F*(A*B) = 2.19**

PASS School Satisfaction

SOURCE	*DF*	*SS*	*MS*
U/C	1	114.8	114.8
Retention/Promotion	1	36.8	36.8
*Interaction(U/C*R/T)*	1	93.7	93.7
Error	56	5168.8	92.3
Total	59	5414.2	

***F*(U/C) = 1.24**
***F*(RetProm) = 0.40**
***F*(A*B) = 1.02**

PASS Confidence

SOURCE	*DF*	*SS*	*MS*
U/C	1	0.6	0.6
Retention/Promotion	1	0.07	0.07
*Interaction(U/C*R/T)*	1	0.27	0.27
Error	56	189.47	3.38
Total	59	190.4	

***F*(U/C) = 0.18**
***F*(RetProm) = 0.02**
***F*(A*B) = 0.08**

Table E-10: Total Clear Types

MMTIC Types Study
Gerry Rentz
University of Alberta

University of Alberta Clinic Referrals 1990-1992

compared with

MMTIC Standardization Group

N = 108

ISTJ	ISFJ	INFJ	INTJ
N = 1 % = 0.93 I = 0.38	N = 6 % = 5.56 I = 1.46	N = 1 % = 0.93 I = 0.67	N = 2 % = 1.85 I = 3.57
ISTP	**ISFP**	**INFP**	**INTP**
N = 3 % = 2.78 I = 0.67	N = 9 % = 8.33 I = 2.41*	N = 23 % = 21.30 I = 2.51***	N = 0 % = 0.00 I = 0.00
ESTP	**ESFP**	**ENFP**	**ENTP**
N = 1 % = 0.93 I = 0.22	N = 15 % = 13.89 I = 0.77	N = 27 % = 25.00 I = 1.04	N = 0 % = 0.00 I = 0.00
ESTJ	**ESFJ**	**ENFJ**	**ENTJ**
N = 7 % = 6.48 I = 1.25	N = 8 % = 7.41 I = 0.46*	N = 5 % = 4.63 I = 1.11	N = 0 % = 0.00 I = 0.00

	N	%	I
E	63	58.33	0.79***
I	45	41.67	1.62***
S	50	46.30	0.81*
N	58	53.70	1.26*
T	14	12.96	0.63
F	94	87.04	1.09
J	30	27.78	0.81
P	78	72.22	1.10
IJ	10	9.26	1.14
IP	35	32.41	1.84***
EP	43	39.81	0.83
EJ	20	18.52	0.71
ST	12	11.11	0.70
SF	38	35.19	0.85
NF	56	51.85	1.36**
NT	2	1.85	0.41
SJ	22	20.37	0.74
SP	28	25.93	0.87
NP	50	46.30	1.29*
NJ	8	7.41	1.13
TJ	10	9.26	1.07
TP	4	3.70	0.31*
FP	74	68.52	1.27**
FJ	20	18.52	0.72
IN	26	24.07	2.02***
EN	32	29.63	0.97
IS	19	17.59	1.27
ES	31	28.70	0.66**
Sdom	23	21.30	0.75
Ndom	30	27.78	1.00
Tdom	10	9.26	0.81
Fdom	45	41.67	1.29

Note: n = 1% of sample. Print date: 2/15/93

* < .05. ** < .01. *** < .001

Base total N = 578. Groups are independent.

Calculated values of Chi Square *or* Fisher's exact probability (underlined)

Type Table Significance

0.49	0.71	1.00	0.18
0.60	5.34	15.92	0.37
0.16	1.07	0.04	0.23
0.30	5.64	1.00	1.00

E	11.33	IJ	0.15	SJ	2.50	IN	11.23
I	11.33	IP	12.40	SP	0.65	EN	0.04
S	4.58	EP	2.51	NP	4.12	IS	1.04
N	4.58	EJ	2.81	NJ	0.10	ES	8.33
T	3.25	ST	1.63	TJ	0.04	Sd	2.30
F	3.25	SF	1.52	TP	0.02	Nd	0.00
J	1.72	NF	7.20	FP	7.82	Td	0.43
P	1.72	NT	0.29	FJ	2.47	Fd	3.53

Table E-11: Total LD Clear Types

MMTIC Types Study
Garry Rentz
University of Alberta

University of Alberta Clinic
LD Referrals 1990-1992

compared with

MMTIC Standardization Group

N = 86

ISTJ	ISFJ	INFJ	INTJ
N = 1	N = 6	N = 0	N = 2
% = 1.16	% = 6.98	% = 0.00	% = 2.33
I = 0.48	I = 1.83	I = 0.00	I = 4.48
¢	¢¢¢¢¢¢		¢¢
ISTP	**ISFP**	**INFP**	**INTP**
N = 1	N = 7	N = 21	N = 0
% = 1.16	% = 8.14	% = 24.42	% = 0.00
I = 0.28	I = 2.35*	I = 2.88***	I = 0.00
¢	¢¢¢¢¢¢¢	¢¢¢¢¢¢¢¢¢¢ ¢¢¢¢¢¢¢¢¢¢ ¢	
ESTP	**ESFP**	**ENFP**	**ENTP**
N = 0	N = 12	N = 20	N = 0
% = 0.00	% = 13.95	% = 23.26	% = 0.00
I = 0.00	I = 0.78	I = 0.97	I = 0.00
	¢¢¢¢¢¢¢¢¢¢ ¢¢	¢¢¢¢¢¢¢¢¢¢ ¢¢¢¢¢¢¢¢¢¢	
ESTJ	**ESFJ**	**ENFJ**	**ENTJ**
N = 7	N = 6	N = 3	N = 0
% = 8.14	% = 6.98	% = 3.49	% = 0.00
I = 1.57	I = 0.43*	I = 0.84	I = 0.00
¢¢¢¢¢¢¢	¢¢¢¢¢¢	¢¢¢	

	N	%	I
E	48	55.81	0.75***
I	38	44.19	1.71***
S	40	46.51	0.81
N	46	53.49	1.26
T	11	12.79	0.53
F	75	87.21	1.10
J	25	29.07	0.85
P	61	70.93	1.08
IJ	9	10.47	1.29
IP	29	33.72	1.91***
EP	32	37.21	0.77
EJ	16	18.60	0.71
ST	9	10.47	0.66
SF	31	36.05	0.87
NF	44	51.16	1.34*
NT	2	2.33	0.52
SJ	20	23.26	0.84
SP	20	23.26	0.78
NP	41	47.67	1.32*
NJ	5	5.81	0.88
TJ	10	11.63	1.34
TP	1	1.16	0.10***
FP	60	69.77	1.29**
FJ	15	17.44	0.68
IN	23	26.74	2.24***
EN	23	26.74	0.87
IS	15	17.44	1.26
ES	25	29.07	0.57*
Sdom	19	22.09	0.78
Ndo	22	25.58	0.92
m	8	9.30	0.81
Tdom	37	43.02	1.33*
Fdom			

Note: ¢ = 1 person. Print date: 2/16/93

* < .05 ** < .01 *** < .001

Base total N = 578. Groups are independent.

Calculated values of Chi Square *or* Fisher's exact probability (underlined)

Type Table Significance

0.71	1.86	0.40	0.13
0.23	4.20	20.17	0.38
0.06	0.85	0.03	0.38
1.24	5.05	1.00	1.00

E	12.54	IJ	0.53	SJ	0.74	IN	13.75
I	12.54	IP	12.21	SP	1.54	EN	0.54
S	3.63	EP	3.57	NP	4.36	IS	0.79
N	3.63	EJ	2.25	NJ	0.82	ES	6.50
T	2.78	ST	1.73	TJ	0.81	Sd	1.48
F	2.78	SF	0.93	TP	0.00	Nd	0.19
J	0.90	NF	5.36	FP	7.57	Td	0.34
P	0.90	NT	0.41	FJ	2.89	Fd	3.81

Appendix F - Clinic Questionnaire

545 DATA SHEET

FILL OUT THIS SHEET THOROUGHLY AND CAREFULLY

Client Name: _____ Adopted: _____ Foster Child: _____

Age: _____ Sex: _____ Grade: _____

Family Background Information

Marital Status:	Single	_____	Separated	_____
	Traditional	_____	Divorced	_____
	Blended	_____	Widowed	_____
				_____
Ethnicity:	White	_____	Asian	_____
	Black	_____	Hispanic	_____
	Native Cdn.	_____	Other	_____

Number of moves within past three years: _____

Alcoholism/drug problems within family system: Yes _____ No _____

Suspected child abuse: Yes _____ No _____

Mental: _____ Physical _____ Sexual _____

Referral Concern

By Whom: _____

Learning Difficulties: Yes _____ No _____

- Reading/Language _____
- Math _____
- Other _____

Behavior Problems: Yes _____ No _____

- Hyperactivity/attention _____
- Conduct Disorder _____
- Emotional/depression _____
- Other _____

Gifted Placement: Yes _____ No _____

ACHIEVEMENT HISTORY

Repeated Grade: Yes _____ No _____

Current achievement level: (Clinical judgement based on data)
Above _____
Average _____
Below _____

TEST DATA

WISC-III (Scaled Score) **or** **SBIV (Scaled Score)**

Verbal Scale

Information	_____	Verbal Reasoning	_____
Similarities	_____	Abst/Vis. Reasoning	_____
Arithmetic	_____	Quant. Reasoning	_____
Vocabulary	_____	Short-Term Memory	_____
Comprehension	_____	Composite	_____
(Digit Span)	_____		

Performance Scale

		PASS	(Raw Score)	(T-Score)
Picture Completion	_____	General Ability	_____	_____
Coding: Part A	_____	Arithmetic	_____	_____
Part B	_____	School Satisfaction	_____	_____
Picture Arrange	_____	Reading/Spelling	_____	_____
Block Design	_____	Penman./Neatness	_____	_____
Object Assembly	_____			
Symbol Search		FULL SCALE	_____	
Part A	_____			
Part B	_____			
Mazes	_____	Validity Indexes	(Raw Score)	
		Response Bias	_____	Q*
VERBAL IQ:	_____	Inconsistency	_____	Q
		Misrepresentation	_____	Q
PERFORMANCE IQ:	_____			
FULL SCALE IQ:	_____			

MMTIC

		TYPE			
Continuous Raw Score	_____	E	U	I	(Circle appropriate)
	_____	S	U	N	
	_____	T	U	F	
	_____	J	U	P	
Dominant Function	_____	E	or	I	(or N/A)

Appendix G - Parent Release Form

University of Alberta
Edmonton
Canada T6G 2G5

Faculty of Education
Clinical Services
1-135 Education North, Telephone (403) 492-3746

CONSENT FOR RELEASE OF CONFIDENTIAL INFORMATION

I, _____ hereby authorize Dr. John G. Paterson, Coordinator of Clinical Services, Faculty of Education, University of Alberta, to forward information concerning myself/son/daughter to:

_____

which by law or otherwise might be considered to be confidential or privileged.

This form or photocopy thereof are equally valid.

SIGNED: _____

WITNESS: _____

DATE: _____